# POLYCRYSTALLINE DIAMOND COMPACT BIT-ROCK INTERACTION

BABAK AKBARI

**Polycrystalline Diamond Compact Bit-Rock Interaction**

by

© Babak Akbari

A Thesis submitted to the

School of Graduate Studies

in partial fulfillment of the requirements for the degree of

**Master of Engineering**

**Faculty of Engineering and Applied Science**

Memorial University of Newfoundland

**June 2011**

St. John's Newfoundland

## ABSTRACT

A physical model of a single PDC (Polycrystalline Diamond Compact) cutter interacting with rock surface is developed, and its most important characteristic is the ability of inputting different force on cutter profiles and outputting cutter penetration. The model is developed in 2 dimensions simplifying the three dimensional cutter movement by a 2 dimensional plane. The model is simulated using the Distinct Element Method and simulation results for the single cutter are interpreted. Simple theories are then proposed to extend the results to a full PDC.

Model inputs encompass parameters such as force profile and horizontal velocity profile on the cutter and also pressure on the rock specimen and the model outputs include dynamic parameters such as cut depth and penetration profile and energy consumed by the cutter.

Relating different types of model inputs and outputs to drilling operational parameters is explained. Approaches to tackle a certain drilling problem relating to the efficiency of particular down-the-hole tools exerting dynamic force profiles on the bit using this model are also explained in detail.

Results show that adding force oscillation generally improves the drilling performance; however, the improvement diminishes as the bottomhole pressure increases. Also, regardless of the force oscillations, the rate of penetration decreases linearly with logarithm of the bottomhole pressure.

## ACKNOWLEDGEMENTS

I would like to extend my deepest gratitude to my graduate supervisors, Dr. Stephen Butt and Dr. Katna Munaswamy, for their time, encouragement, dedication, and support of my research activities. Dr. Butt provided significant insight into the nature of the problem and his perceptive abilities and timeliness helped me overcome many obstacles on the road to completing this work.

I dedicate my sincere thanks to Farid Arvani, project manager, for his time, encouragement, and endless support. Without his encouragement and ideas this work would have never been completed.

I would like to thank the Atlantic Canada Opportunity Agency (AIF Contract no. 781-2636-1920044), Husky Energy, and Suncor Energy for funding this research over the past two years. Additionally, the financial and academic support of the Faculty of Engineering and Applied Science is graciously acknowledged.

Thanks to Sacha Emam for his assistance with the simulation code and also Derek Chechak for proofreading the thesis and helping me with citations.

I would also acknowledge Moya Crocker for her outstanding service to all the graduate students and also faculty.

# Table of Contents

## List of Tables

## List of Figures

## List of Symbols, Nomenclature or Abbreviations

| | |
|---|---|
| ADG | Advanced Drilling Group |
| ALE | Arbitrary Lagrangian-Eulerian |
| BHP | Bottom Hole Pressure |
| $C_t$ | Cut depth at time t |
| $\overline{Ct}$ | Average cut depth at time t |
| $\overline{Ct_f}$ | Final average cut depth |
| DEM | Distinct Element Method |
| F | Force per unit thickness of cutter |
| FEM | Finite Element Method |
| $F_n$ | Normal contact force |
| $F_{s,max}$ | Maximum allowable shear contact force |
| $F_x$ | Horizontal force acting on the cutter |
| $F_y$ | Vertical force acting on the cutter |
| ME | Mechanical Energy |
| MRR | Material Removal Rate |
| $MRR_f$ | Final Material Removal Rate |
| MSE | Mechanical Specific Energy |
| P | Force oscillation percentage |
| PDC | Polycrystalline Diamond Compact |
| PFC-2D | Particle Flow Code in 2 Dimensions |
| R | Cutter center's distance from the bit center |

| | |
|---|---|
| ROP | Rate of Penetration |
| RPM | Round Per Minute |
| T | Cutter thickness |
| TBM | Tunnel Boring Machine |
| TOB | Torque on Bit |
| TVD | True Vertical Depth |
| UCS | Uniaxial Compressive Strength |
| VARD | Vibration Assisted Rotary Drilling |
| $V_x$ | Horizontal velocity of cutter |
| $V_y$ | Vertical velocity of cutter |
| WOB | Weight on Bit |
| $WOB_{static}$ | Static Weight on the Bit |
| 2-D | 2 Dimensional |
| 3-D | 3 Dimensional |
| $d\varepsilon_{ij}^{p}$ | Plastic strain increment component |
| $d\lambda$ | Scalar not specified by flow function, determining plastic flow |
| f | Frequency of force oscillations |
| $h_{ij}$ | Tensor function, determining the plastic strain tensor |
| t | Time elapsed from the simulation |
| $\varepsilon_{ij}$ | Total material strain tensor |
| $\varepsilon_{ij}^{e}$ | Elastic strain tensor |
| $\varepsilon_{ij}^{p}$ | Plastic strain tensor |

| | |
|---|---|
| $\lambda$ | Cutter side rake angle |
| $\mu$ | Friction coefficient between particles |
| $\pi$ | Pi number, the ratio of circle's perimeter to its diameter |
| $\sigma_{kl}$ | Stress tensor |

## List of Appendices

# 1 Introduction

*"Life leaps like a geyser for those who drill through the rock of inertia."*

*Alexis Carrel*

The urge and desire to exploit and take control of the universe has been humanity's instinct for centuries. The invention of aircraft is an impressive attempt of man empowered by this instinct. Man has understood since his existence that in order to survive he has to think beyond the limits of what can be seen by the naked eye and act accordingly. This ability and instinct of humans made them superior to the rest of the creatures on Earth and put them in a position to develop a kingdom on the earth and exploit nature.

This instinct did not just make us explore space and upper levels; it also made us wonder that if we can get to the places under our feet. The attempts of a child to dig down into the ground in the house garden probably initiates from that very inherent desire. Long story short, humans started to mine and exploit the minerals and water and then they found out that the deeper it goes the more exciting and richer the mother earth becomes. The Chinese used very basic digging tools mounted on a basic derrick; they dropped a weight on a certain spot on the ground and removed the crushed rock resultant of the impact and repeated the process over and over again to dig holes tens and later hundred meters deep. Those very basic drilling systems were developed and advanced over centuries and now, at the time of authorship of this thesis, this industry is one of the most prolific and advanced industries to which the petroleum industry is inextricably dependent.

Nowadays, we are able to have photos and movies from inside wells of several thousand meters in depth. We can lead a bit down the ground, make complicated well geometries, and hit predefined spots several kilometres down with accuracy comparable to a professional golfer. We inject extra gas down the earth into the permeable formations and produce it later when needed. We made the earth not only a place to extract things, but also a place to store things. We tamed our (relatively) new slave and prevented her from blowing out and showing her anger from trespassing her long lasted virgin territory. Never successful in suppressing our other powerful instinct, greed, we get defeated by this anger and that results in disasters such as the one in the Gulf of Mexico in 2010, which destroys our very first home, the Earth's surface.

Not being able to even think about compromising the benefits gained from the black fluid produced from deep within the Earth, we try to advance our technology to address environmental concerns while continually developing our drilling techniques to overcome and exploit harsher, harder, and more aggressive targets.

This industry gained power by impressive improvements in drilling methods and the introduction of advanced drill bits and mud circulation systems. Consequently, it became feasible to reach targets that were considered completely impractical not long ago.

All these improvements, especially those related to drill bits, regardless of all the progressions in the industry, were not based on a structured and firm theoretical basis. Intuition, imagination, and experimentation were three primary and powerful tools used by those who made these advancements happen. The invention of PDC (Polycrystalline Diamond Compact) bits and their rapidly growing acceptability in this industry is a good example. Not much is known about the real mechanism by which the rock fails under the cutting action of these bits, but surprisingly, every day we see more advanced and efficiently designed PDCs introduced to the industry.

This makes us wonder how efficiency could be improved if we knew the real mechanism of action of the PDC bits in the ground. A smallest insight in the mechanism explains an exceedingly large number of why's even though we have answered a lot of how's without the need to answer those why's. Knowing the 'why', has made us who we are. As Diane Ravitch stated, The person who knows 'how' will always have a job. The person who knows 'why' will always be his own boss.

Obviously, the complexity of the problem is the very first hindrance in the commencement of such a study. Imagining a real PDC bit rotating down the hole might be easy, but even imagining it in contact with the rock and the consequential rock cutting action gives some clues about how complex the problem can get. The nature of the contact between the individual cutter and the rock, and the interaction of all these entities with each other is a requirement.

Simplifying the problem can be a first step to tackle the bigger mystery. One approach to the simplification could be looking at an individual PDC cutter action. In three dimensions, even this simplified problem is very complicated and cumbersome to reproduce either experimentally or numerically.

The simplified case of the action of the PDC cutter with rock surface in two dimensions is the answer. Numerous researchers have reproduced that scenario over time, and drew lots of useful conclusions from their results that both answered a lot of questions and raised new ones. Not very long ago, researchers attempted to reproduce the problem numerically and this has been advancing ever since. Thanks to the introduction of very sophisticated and specialized numerical simulation methods, these simulations were developed with greater ease, realism, and power in representing the real physics and nature of the problem.

This thesis reports on a very small attempt made to simulate this interaction. It is inspired by and builds on the aforementioned works, and the author hopes that this answers some of the questions that are currently unanswered. However small and brittle, it represents one brick in the process of building this palace of knowledge.

Previously done work are described in Section 2 which include rock failure models and then cutting models and then numerical simulations. In Section 3 the justification for the choice of a certain numerical simulation method over the other methods is given. In the next section the model is physically described and the numerical interpretation of that is given and then in Section 5 the input parameters to the model are described and their physical interpretations are discussed and the outputs are the topic of the next section, where their physical interpretations are discussed and also extension of their results to full PDC bits are proposed. In Section 7 the simulation results are discussed and finally some recommendations for the work following up this are given in Section 8. The logical sequence of the current work, from model description and solution options to the solution interpretation methods and results, coincide with the chronological order of the work and chapters.

### 1.1 Contribution of the Thesis

Answering the basic question of the effect of different loading regimes on the bit on drilling efficiency and, in particular, rate of penetration requires a cutter-rock interaction model capable of solving the stated problem.

The question arose as an attempt to justify the efficiency (if any) of a hypothetical down-the-hole tool providing oscillatory changing force in the drill string that transmits to the bit and superimposes on the constant force on the bit (called Vibration Assisted Rotary Drilling tool). The design of this tool is highly dependent on the answers to the question that if this mechanism is effective, what is the best force profile that results in the highest drilling efficiency? Knowing the answer to this question, the tool design recommendation could be given for the most optimized drilling performance.

# 2 A Review of Rock and Cutting Models and Simulations

As an essential part of the work, a thorough review of related literature was done. The logical sequence of this literature is to first gain insight into rock constitutive models and failure modes and mechanisms, without which a review of rock cutting models is hard to understand. Finally, a review of simulation of some proposed models will be the final part of a review into the literature of rock cutting modeling and simulation.

The chronological order of the actual literature review was also coincident on the logical order and was done during the first year of the program.

## 2.1 Rock Failure Models

Rock failure is the phenomenon of breakage under certain loading conditions. Failure criteria define and describe the loading conditions under which the rock starts to fail. The importance of failure criteria in drilling penetration mechanisms investigation is obvious; no penetration occurs as long as no rock failure occurs. An understanding of what really happens to the rock under load and how that causes the rock failure is the most helpful tool in the assessment of drilling penetration mechanisms, since it enables the researcher to visualize the real situation down the hole where the actual drilling takes place.

Rock failure behavior is an extremely complicated phenomenon if it has to be described completely. This is because of the non-homogeneous rock nature and its granular structure. Other solids such as metals do not have such granular structures and their macroscopic behavior is, to a good extent, indicative of their microscopic behavior.

In addition to the failure criteria itself, the post failure behavior of the rock is of great importance when it comes investigating penetration mechanisms. The fact that how the cutting is generated and how different loading conditions might affect the post failure behavior of the failed portion of rock influences the mechanisms involved in penetration. Different proposed rock failure criteria are described in the first part of this subsection, and the second part describes post failure behavior and proposed models.

### 2.1.1 Failure Criteria

Mohr's criteria [1] is the most famous and widely used one among all the others. The criteria in its very preliminary form needs three parameters to be fully defined. Friction angle, cohesion and tensile strength are the parameters which can define a linear Mohr-Coulomb failure envelope. The physical assumption made to develop this criteria was that the larger the hydrostatic component of the stress, the larger the stress required to cause the rock failure. The amount of this sensitivity of failure load to hydrostatic load is indicated by the friction angle.

The criteria are usually defined in shear-normal stress space; however, it also has representations in principal stress space [2]. Also, it has simpler alternatives such as Tresca's criterion, for example, which is the same as Mohr-Coulomb except that it assumes no friction angle [3]. On the other hand, more sophisticated versions of Mohr-Coulomb introduce curved failure envelopes with a parabolic equation. Such an envelope requires three parameters and does not need a separate value for tensile strength as the intersect of the envelope with the horizontal axis should be the tensile strength [4]. Figure 2.1 shows the three versions of the criteria in Shear-Normal stress space.

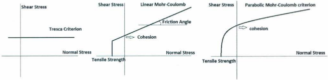


**Figure 2.1: Different failure envelopes from Mohr`s theory.**

The parabolic envelope practicality has proven to be much better than even the linear one, especially for the studies of rock indentation and penetration mechanisms. A much better match with experimental data was obtained using the parabolic failure envelope [5].

The aforementioned failure criteria are independent of the intermediate principal stress. They just rely on the major and minor principal stresses and not on the value of intermediate principal stress. This is true to some extent, but the intermediate stress also plays a role in failure and the failure is not completely independent of it.

There are failure criteria which are dependent on the intermediate principal stress. The simplest one is Von Mises criteria [6] which is often used to describe metal failure. The representation of this criteria is a cylinder centered around the hydrostat line in the 3-D principal stress space. This criteria is in one aspect similar to Tresca, in both cases the failure stress does not depend on hydrostatic pressure. A hydrostatic pressure dependent criterion is that of Drucker Prager [7] which its representation in the principal stress space is a cone centered around the hydrostat. The cone shape means that the failure stress might differ depending on the amount of hydrostatic stress. Obviously, the base of the cone faces toward the low hydrostatic pressures (and in fact, the so-called hydrostatic tension).

Figure 2.2 shows the two criteria in principal stress space.

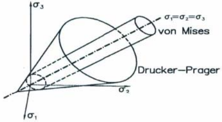


**Figure 2.2: Drucker Prager and Von Mises criteria (after Fjaer et al. [9]).**

Characterization of materials and determination of their failure parameters is typically done by certain types of tests among which the Triaxial test is the most useful one [8]. The test device exerts axially increasing load on the rock core sample and the sample is being confined hydrostatically from the sides. Stress-strain curves are extracted from the strain gauges measurements and the yield point and maximum bearable load on the rock are monitored.

Several Mohr's circles at failure plotted in the shear-normal stress space can determine a failure envelope which is the common tangent to all of the Mohr's circles at failure.

### 2.1.2 Post Failure Behavior

As mentioned before, the post failure behavior of the rock is the part that really describes the rock behavior at failure point and after that. Plasticity and related strains are the factors that determine how the rock is going to behave after meeting the failure criteria. The theories and models proposed for this purpose are categorized as plasticity theory.

The main point in all the plasticity theories is the addition of plastic strains to the elastic formulation of stress and strain.

$$\varepsilon_{ij} = \varepsilon_{ij}^{e} + \varepsilon_{ij}^{p} \tag{2.1}$$

In which $e$ refers to elastic strains and $p$ refers to plastic strains. The major difference between these two types of stresses is that when the stress is relieved the elastic strains will be recovered while the plastic strains still remain unrecovered and permanent [9].

The plastic strain can be determined using the theories developed and called as flow rule. The basic equation for flow rule is given as [9-10]:

$$d\varepsilon_{ij}^{p} = d\lambda\, h_{ij}(\sigma_{kl}) \tag{2.2}$$

In which $d\lambda$ is a scalar and $h_{ij}$ is a function of stresses. The important point about this equation is that plastic strain increment does not depend on stress increment but depends on the stress itself.

Drucker [11] suggested a function called flow potential, in which partial derivation of this function with respect to each stress component gives the corresponding $h$ function. If this function is the same as the yield surface in the stress space (failure envelope) then the flow rule is called associated; otherwise, it is called non-associated.

As an example of how associated flow rule works, the Mohr failure envelope can be considered. By plotting the envelope in a 2-D principal stress space, and also visualizing the axes to be also the corresponding principal plastic strain increments, an arrow perpendicular to the failure envelope line represents the plastic flow in terms of its two principal value increments. (Figure 2.3)

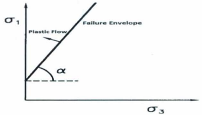


**Figure 2.3: Mohr-Coulomb envelope in principal stress space and associated plastic flow rule (after Fjaer et al. [9]).**

The angle $\alpha$ is directly proportional to the friction angle. Interpretation of the associated flow in shear-normal stress space is also available. For the case of Mohr-Coulomb, dilatant behavior will be observed in the flow – which means that the rock tends to dilate, expand in volume, under shear stress – if the friction angle is positive. For negative friction angle contractant behavior of the plastic flow is observed (opposite to dilatant) and for friction angle of 0, which is the Tresca criterion assumption, incompressible flow is observed.

Non-associated plastic flow is the case when the flow potential function is not determined using the yield surface. Several authors developed and proposed different models for non-associated flow rules which are out of the scope of this review [12].

### 2.2 Rock Cutting Models

Rock cutting models attempting to simulate the response of rock interacting with the drill bit have been developed by several authors. The common aspect of almost all of these models is that they considered a single cutter interacting with the rock surface for the case of a PDC bit.

A constant depth of cut is considered and the cutter moves with constant horizontal velocity, representing the rotary motion of the single cutter on the PDC bit. Some models emphasize the geometrical aspects of the cutter, such as back rake angle, chamfer, etc., while others focused on the role of rock failure mode in various situations. Alternatively, there are models focusing on the type of rock and its impact on drilling process.

The simplification of considering only a single cutter is reasonable as the behavior of the full PDC bit could be an average of the individual cutters' actions. There is no interaction between the performance of individual cutters as they are parts of an approximately rigid body (compared to rock).

Zeutch and Finger [13] made a series of experiments in an attempt to correlate the response of the rock with the cutter movement, and generation of crack and chip. They found that mechanism of chip generation is different depending on the cutter geometry and rock properties and other parameters. The common point is that the fractures in the rock that cause the chip formation mostly nucleate from the cutter tip, and these fractures grow to the rock surface (Figure 2.4). A zone of crushed rock material is also formed in front of the cutter. The crushing mechanism and chipping mechanism are different; this is one of primary concepts and will be discussed in more details later.

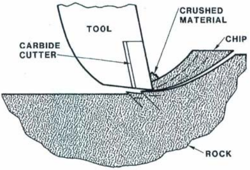


**Figure 2.4 Schematic of single cutter in contact with the rock (after Zeutch and Finger [13]).**

Hareland and Rampersad [14] developed a model predicting the behavior of drag bits based on operational conditions as well as bit geometrical specifications and design, and also rock constitutive law. The model predicts rate of penetration and bit wear rate based on the input parameters. The model was developed on the basis of a single cutter interacting with the rock, and the experimental and field verifications were successful.

In a similar study, Jogi et al. [15] made a completely analytical model investigating the response of a single PDC cutter cutting rock with constant depth of cut. He used a Mohr-Coulomb failure criteria in the model development (refer to section 2.1.1) to characterize the shear plane formed as a result of cutting process. The same shear planes were observed in the experimental work of Zeutch and Fingerr [13]. They derived expressions relating drilling rate of penetration, specific energy, and cutter wear rate to cutter design, drilling operational conditions, and also rock constitutive law. Figure 2.5 shows a schematic of the model and its boundary conditions. Bottomhole pressure is also one of the factors considered in the model; it can easily be seen as the uniform pressure exerted on the rock surface. Some authors [23, 24] suggested that in these single cutter-rock interaction models the assumption of linear elasticity is a reasonable approximation in case of hard rocks.

Poor performance of PDC bits in shale was a big concern in the early days of this technology development. A lot of theories and attempts were made to improve the efficiency of PDC bits, especially in drilling shale formations. Knowlton [16] proposed a modified design of PDC cutter with positive rake angle which overcame the difficulties encountered in drilling shale formations. As explained in the paper, the main reason of poor performance is due to shale swelling due to contact with the water phase of the drilling mud.

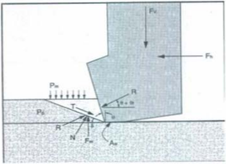

**Figure 2.5: Single PDC cutter in contact with rock surface (after Jogi et al. [15]).**

A more sophisticated model was proposed for cutter rock interaction by Gerbaud et al. [25] adding more complexities to cutter geometry and incorporating the chamfer made on some PDC cutters for better drilling efficiencies. They claimed in addition to forces acting on the cutter in the front face, there are forces acting on the cutter back, which has been demonstrated [26, cited in 25] using an elasto-plastic rock behavior model. Figure 2.6 shows a schematic of their model general parameters. Their model has also been in good agreement with experimental cutting tests.

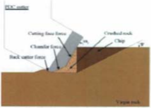


**Figure 2.6: Three different categories of forces introduced on the single PDC cutter, cutting face; chamfer; back cutter forces (after Gerbaud et al. [25]).**

Not all the cutter-rock interaction models are developed in 2-D. For example, Behr et al. [17] developed a 3-D drilling model which was inspired from a 2-D modeling approach and incorporated the geometrical considerations into a 3-D model. Warren [20] also incorporated results of 2-D rock cutting models into four different spatially designed PDC bits and investigated their relative performance.

A phenomenological model was also proposed for the performance of drag bits [28]. The beginning hypothesis of their work builds on a suggestion made earlier in the literature review [29] that bit-rock interaction is characterized by the coexistence of two processes: cutting of the rock and frictional contact underneath the cutter. The torque on the bit (TOB) and weight on the bit (WOB) can thus naturally be decomposed into two components, one associated with the cutting action and the other with the frictional contact. Their model does not constitute a complete drilling response, but it does provide a constraint between drilling parameters including WOB and TOB. They concluded that any model that aims to predict the response of a full PDC bit has to take the forces acting on a single cutter into account.

As mentioned previously, in addition to theoretical models, experimental models were developed for single PDC cutter interacting with rock. These experimental set ups were employed to gain insight into the real mechanisms of PDC bit penetration. One of the early works of this type was done by Zijsling et al. [18] in which a single PDC cutter cut the rock under simulated bottomhole pressure. Their main focus was in the cutting of shale formations and they made use of two different types of shale. Figure 2.7 shows a drawing of their single cutter tester apparatus in which the cutter is attached to a vertical rotating shaft.

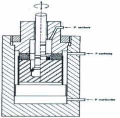

**Figure 2.7: Single PDC cutter experimental simulator (after Zijsling et al. [18]).**

Other experimental investigations were performed for the specific purpose of investigating the effect of back rake angle on the cutting process [21]. Back rake angle is defined as the angle between the cutter face normal vector and the cutter velocity vector projected in a vertical plane, which includes the cutter velocity vector. The side rake angle is defined as the same angle projected in a horizontal plane [27]. Hareland et al. [22] also developed a single PDC rock cutting analytical model investigating the effect of cutter rake angle on the single cutter efficiency. They proposed a new parameter representing cutting efficiency called specific volume, which is the ratio of the volume removed by the cutter in a major chip to the maximum force required to remove that much volume. Other researchers [27] have also investigated the effect of back and side rake angles in cutting efficiency and force on the cutter. They made a series of experiments with sharp PDC cutters without chamfer, and by changing side and back rake angles. They found out that the effect of side rake angle is negligible in the resultant force acting on the cutter and therefore the friction factor between the cutter and the rock. They concluded that proper selection of back and side rake angles can affect drilling efficiency and also bit steerability. Figure 2.8 shows the back and side rake angles illustrated on a single PDC cutter.

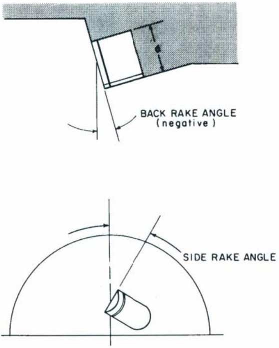


**Figure 2.8: Back rake angle and side rake angles illustrated (after Bourgoyne et al. [64]).**

Models developed on the basis of experimental single cutter tests are also available. Glowka [19] made use of experimental single PDC cutter tests and analyzed the data to propose a model for forces on the cutter correlated with the depth of cut and cutter angle and rock physical properties. He also investigated the effect of nozzle fluid velocity and incorporated that into the model, since the experiments were carried on with a nozzle jet which was mounted in the set-up mainly for cutting removal purposes. Rafatian et al. [30] also conducted an experimental study with their pressurized single cutter testing apparatus. Their set-up is very similar to setups in other studies that performed single cutter testing. An important feature of their experimental set-up is that it is capable of simulating bottomhole pressures as high as 950 psi (6.5 MPa). The cutter is mounted on a shaft which rotates and scratches the rock underneath in the circular path that it travels.

Force transducers measure vertical and horizontal force components during the tests, which are used later in determining drilling mechanical specific energy (MSE). MSE is a concept introduced and used for the first time by Simon [31] and later by Teale [32], which claims to be a preferable alternative to rate of penetration when assessing and measuring the drilling efficiency. The exact definition of this quantity is the energy consumed to remove a unit volume of rock. Rafatian et al. [30] found out that the specific energy increases dramatically when the bottomhole pressure increases even by a small amount from the atmospheric pressure. The reason is suggested to be a fundamental change in failure mode from brittle to ductile and therefore a decrease in the efficiency of cutting. In the ductile mode, no chip forms and cuttings take the shape of a ribbon stuck to the cutter wall pushed to the wall by the bottomhole fluid pressure.

In addition to studies based purely on mechanical aspects of cutter-rock interaction, Detournay and Atkinson [33] investigated the effect of pore and bottomhole pressures and incorporated them in a simple mechanical cutter model, introduced earlier by Merchant [34], for the cutting of metals. They coupled an analytical mass balance and diffusion with the failure model and used the equation for specific energy developed by Merchant [35]. The equation stated that the MSE is neither merely a function of bottomhole pressure or differential pressure (the difference between the pore pressure and bottomhole mud pressure), but is a function of the difference between the bottomhole mud pressure and the pore pressure in the plane of shear failure. They identified different drilling regimes, and in one called High Speed Regime, the pore pressure in the shear plane is essentially zero due to lack of time for the fluid in this plane to equilibrate with the formation fluid and the expansion of the pore fluid in the shear plane due to shear dilatant behavior of the rock [36]. This regime is expected in high RPM drilling and also low permeability rocks such as tight shale. In the other extreme, low speed regime, the pore pressure in the shear plane equilibrates with formation pressure and the MSE becomes a function of the differential pressure. Figure 2.9 shows the cutting model they used and the shear failure plane.

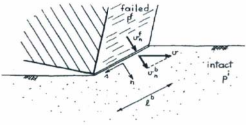


**Figure 2.9: Cutting model used and the location of the plane of shear failure (after Detournay and Atkinson [33]).**

Peltier and Atkinson [37] made another analytical study looking into the effect of filtration rate of mud into the formation and also rate of penetration and the consequential pore pressure changes underneath the bit. The importance of these studies in the investigation of penetration mechanisms is due to the fact that rock pore pressure affects the ease of rock breakage. The higher the pore pressure the easier the rock to fail all the other conditions remaining constant. The reason was discussed by Terzaghi [38] introducing the concept of effective stress based on empirical observations. The rock effective stress is defined as the stress state identified by the two principal stresses subtracted from the pore pressure [39]. This shifts the Mohr's circle discussed in section 2.1.1 to the left and makes the rock more likely to break.

### 2.3 Rock Cutting Numerical Simulations

Recently, by development of mechanical simulation software utilizing different algorithms such as finite element or discrete element method to model solids and fluids and their mechanical response due to loading (mechanical, thermal, etc.), it is much more convenient and reliable to replace analytical solutions with their numerical equivalent.

In the previous section, several analytical approaches to solve the cutter-rock interaction problems were introduced and their methods and their applicability were discussed. In this section, a brief review of the attempts made to numerically investigate this problem will be presented. This part of the literature review will be presented in a chronological manner as the numerical simulation methods are relatively new concepts.

The earliest work done in numerical simulation of cutting action of drag bits dates back to 1984 when Victor and Kleinosky [40] studied chip formation in rock under a line load and in front of a drag bit cutter. The analysis was accomplished using a special purpose interactive graphics finite element code, SICRAP, written for the simulation of mixed mode crack propagation under linear elastic fracture mechanics assumptions. The first study provided some interesting qualitative results, and in the second study, correlation with experimental tests on chip formation by drag bit cutter in Berea sandstone was found to be very satisfactory. According to the authors, the elastic analysis, coupled with fracture mechanics, is capable of modeling rock cutting. Figure 2.10 shows the model schematic and meshing before and after deformation.

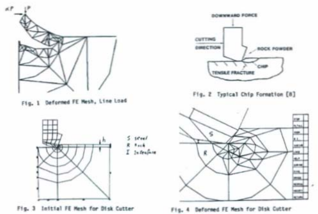


**Figure 2.10: Full model and meshed model before and after deformation (after Victor and Kleinosky [40]).**

In 1994, Pierry et al. [41] used finite element method to simulate cutting action of a single PDC cutter under simulated bottomhole pressure. They identified shear planes of failure based on two different strain localization criteria and found that breaking occurs by strain concentrating in a thin area called shear band. Figure 2.11 shows different strain localization patterns observed by them based on different criteria they used. Bifurcation criterion is based on the Rice analysis [42] (top left part in Figure 2.11 is an instance), scalar indicator criterion based on von Mises strain field (two parts on the right), and finally the Drucker-Prager constitutive law (top right part of the Figure). For all the cases, the existence of a plane of localized strain (called plane of shear failure) is apparent. One year later in 1995, the same author and Wang et al. [43] confirmed these results in a similar study with finer meshes and more precise constitutive laws.

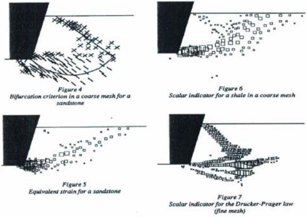


**Figure 2.11: Strain localization patterns with different materials and criteria (after Pierry et al. [41]).**

In 1999, Huang et al. [44] performed the preliminary attempt to simulate rock cutting process using the Discrete Element Method (DEM). Their focus was in reproduction of two different failure modes, brittle and ductile, observed in low and high pressure drilling environments respectively (refer to section 2.2) [30]. Their simulations successfully yielded the results observed experimentally by assessing the cuttings morphology. In 2005, Gong et al. [45] performed a series of numerical simulations using the DEM to explore the effect of joint orientation on rock fragmentation process by a tunnel boring machine (TBM). They observed crack initiation patterns and drew conclusions on changes in stress field and tool performance with respect to joint orientation.

In 2006, Han and Bruno [46] attempted to simulate the mechanism of rock breakage in hammer drilling. Hammer drilling uses percussive impacts with a specially designed percussive bit and is known to be an efficient drilling method in hard rock drilling [47]. They used a Mohr-Coulomb material with strain softening in an explicit finite element model. They also defined fatigue criteria to account for the failure occurred due to cyclic loading of the percussive impacts. Their numerical simulations generated three outputs: a plot of failure advancement, a history of rock failure, and a history of rock fatigue/damage. Another important and distinctive feature of their model was that they applied lateral confining stresses to the model lateral boundaries instead of constant displacement and this simulates the real world underground stress much more accurately [48]. Refer to Figure 2.12 for model configurations and details. A few months later, the same authors [49] calibrated laboratory and full scale mud hammer at depth and simulated borehole and in situ conditions. Their studies have significantly advanced the fundamental understanding of the penetration mechanisms of hammer drilling.

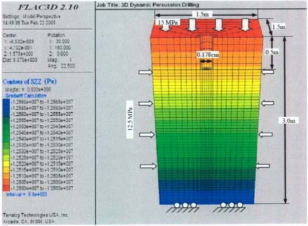


**Figure 2.12: Finite element mesh for rock cutting and its boundary conditions (after Han and Bruno [46]).**

In 2008, Tulu et al. [50] developed an explicit finite element model simulating a single rigid cutter cutting a cylindrical rock specimen in a circular path on its surface. Their early simulation results measuring vertical and tangential load during the course of simulation seem to be working and giving realistic results. One year later, in 2009, the same authors in another paper [51] published the results of their numerical simulations calibrated with single cutter experimental test data which was published before by Glowka [19] (refer to section 2.2). Their model, after modifying several key parameters such as tensile strength, matched the experimental tests results (force profiles acting on the cutter). In their conclusion, they suggested that strain localization appears to be mesh-dependent and therefore the validity of this finite element model is uncertain.

In 2009, Block and Jin[52] conducted a very interesting study on the failure mode of rock and bottomhole pressure using the Distinct Element Method. This study was inspired by the aforementioned work done in 1999 by Huang et al. [44]. They confirmed the previous results of ductile and brittle failure modes [44, 30] in high and low bore hole pressure conditions. Their method differs significantly from previous studies in that grain-level forces were spatially averaged to determine the rate of energy dissipation within the rock volume during the entire cutting process. Their results show that there is a direct and quantifiable relationship between confining stress, down-hole pressure, drilling efficiency and a transition from chip-like (brittle failure) to ribbon-like (ductile failure) cuttings morphologies. Figure 2.13 shows how these failure modes look like. Creation of a chip cutting is obvious in the left side where the failure is in brittle mode.

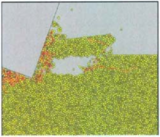
**Brittle failure in 0 MPa bottomhole pressure**

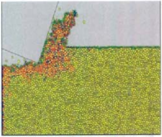
**Ductile failure in 30 MPa bottomhole pressure**

**Figure 2.13: Two different failure modes observed in a distinct element simulation (after Block and Jin [52]).**

In 2010, two very impressive single cutter-rock interaction simulations works were published. Jaime et al. [53] compared various approaches in explicit finite element modeling from Eulerian and ALE formulation to Lagrange formulation and found out that the last one is suitable for their study. The results of a Lagrangian FEM in modeling rock cutting gave them excellent matches to experimental single cutter tests as it can also be seen in Figure 2.14.

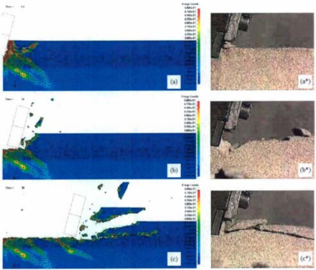


**Figure 2.14: Laboratory rock cutting test (right side) compared to numerically simulated version (right side), 3.6 depth of cut, countours show damage values (after Jaime et al. [53]).**

In another study [54] particle crushing effects were incorporated into discrete elements. Adding the effect of particle crushing in the model made the model to match the laboratory experiments better. Particle crushing was found to play a significant role when a rock had a relatively high strength or high stiffness. However, from the cutting force perspective, crushing of particles does not seem to significantly affect the resulting force.

Having a general picture of previously done work in the area of PDC cutter-rock interaction, the numerical attempts described in section 2.3 will be evaluated in the next chapter.

# 3 Evaluation of Numerical Simulation Methods

This chapter is devoted to summarizing the early attempts that were made to evaluate possible rock cutting numerical simulation methods. This process included a literature review, basic simulation efforts, and observance of their effectiveness towards simulating the desired scenario. Three conceptually different numerical methods were investigated during this process: the finite element method (implicit formulation); the finite difference method (explicit formulation), and, the distinct element method (explicit formulation). This presented order also coincides with their chronological order of investigation and, interestingly, their effectiveness.

## 3.1 Finite Element Method (Implicit Formulation)

### 3.1.1 Overview

The very first numerical methods for the analysis of solids were based on the finite element method with an implicit formulation.

In the finite element method, the solid is discretized into finite elements using an appropriate meshing scheme. Each individual element is the smallest unit in the finite element model and unit stresses and displacements will be defined for each element. A finite element solution will be a new stress field and displacement field after application of a loading on the body. For the purposes of this investigation, the finite element methods are categorized into two different classes of implicit and explicit.

In the implicit solution method, a matrix known as global stiffness matrix is formed which is an assembly of all the individual stiffness matrices of each single element. The term "stiffness matrix" means a matrix whose product with the stresses acting on the elements will result in consequent strains on that element. Therefore, a given stress field gives rise to a resultant strain field which determines the deformed shape of the material. The stiffness matrix is a function of the mechanical constitutive law by which the material is defined.

The implicit method means that this method does not give a solution by directly solving the equations of motion, but rather by solving the equation of stiffness matrix using iteration techniques. The higher the number of elements, the bigger the stiffness matrix and the bigger the computational effort needed to solve the resultant equation. Interested readers are referred to the textbook given in the Reference [55] for a thorough discussion and introduction to the basics of this method.

### 3.1.2 Features of the method

The main feature of the implicit methods is that the time step required to solve a given loading condition can be arbitrarily large, but even so, the method will still give unconditionally stable solutions to the problem. This is the main advantage of this method compared to explicit methods, as will be explained later, in which a maximum allowable time step size limit increases the required computational efforts.

Another feature is that numerical damping of energy is inherently within the solution and is dependent on the time step; resultantly, it will give unconditionally stable solutions despite other methods in which no significant damping algorithm is available for a dynamic solution.

The issues addressed above are the main advantages of the implicit finite element method when compared to other methods. There are a few more minor advantages which are out of the scope of this investigation's objectives.

### 3.1.3 Limitations of the Method

The major disadvantage of this method, however, is that time steps could be arbitrarily large, but a large amount of computation effort is required for each individual time step. The reason for this, as mentioned in section 3.1.1, is due to the iterative solution scheme that might require a large number of iterations to converge the final solution.

The other issue regards nonlinear constitutive laws defined for materials. As the complexity and nonlinearity of the material constitutive law increases (which is always the case for rock), extra iterative procedures are required to follow the nonlinear constitutive law.

Among the disadvantages, there is the problem of stability of path-sensitive problems. For these problems the stability of the solution should be demonstrated and it should be proved that the material has followed a physically stable path. (Path-sensitivity includes materials with a hysteresis behavior, where almost all rocks demonstrate a strong version of this behavior ) [56].

Another disadvantage is that an additional computing effort required for analysis of large displacement and large strain problems (all the rock cutting models involve very large strains due to failure and flow of the rock) [55].

### 3.1.4 Conclusion

Considering all the information discussed above regarding the nature of the method and its pros and cons, the following conclusion regarding its applicability was drawn. Rock cutting numerical simulations have two major characteristics which render them unique from other physical phenomena being used in implicit simulations (such as metal deformation). First, the constitutive laws governing the rock behavior are extremely nonlinear and also demonstrate strong hysteresis behavior (refer to sections 2.1.1 and 2.1.2). Second, the rock cutting process is a large strain problem, large deformations take place in the shear plane of failure (refer to sections 2.2 and 2.3).

Taking a look at section 3.1.3, it is obvious that these two main distinctive characteristics of rock cutting process fall exactly into two main weak spots of implicit methods. As it will be explained later, these two are, in contrast, the main strengths of explicit methods.

As a conclusion, the utilization of implicit FEM has proved to be extremely inefficient and probably ineffective for our purposes.

## 3.2 Finite Element Method (Explicit)

### 3.2.1 Overview

The explicit solution of the finite element method (sometimes called finite difference method) is still based on discretization of the solid body with a finite element mesh. However, for the explicit solution no global stiffness matrix forms as it was the case for the implicit formulation [57]. The explicit method solves the dynamic equation of motion over each time step, and then the new velocities and displacements give the new strain field. In turn, the new strain field is converted to the new stress field using the constitutive equations, and these give new forces acting on elements that will again be inserted into the dynamic equation of motion. This cycle continues for as many time steps as required. Figure 3.1 illustrates this cycle.

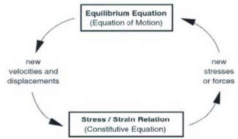


**Figure 3.1: Calculation sequence in an explicit FEM method.**

There is one important consideration regarding the validity of the solutions given by explicit methods. Looking into the calculation cycle, when the stress field changes, the strains should change accordingly; but they do not. This suggests that the explicit simulations might not be realistic; however, if the time step chosen for calculation cycles is sufficiently low that the information physically does not have the time to pass from one element to the other, the simulation results would be valid. This minimum time step is called the critical time step and depends on the smallest element size and also the speed of wave propagation inside the material being modeled.

### 3.2.2 Features of the method

The main feature is that however small the critical time step (refer to section 3.2.1) might need to be, the computational effort per each cycle is much less than the implicit method. The reason is that there is no matrix to be solved, and therefore, no iteration is needed. Also, despite the implicit method, any constitutive law with any degree of nonlinearity and complexity can be incorporated into an explicit formulation without adding up to computational effort since all the constitutive equations are directly applied to the already known strains and give the new stresses (refer to section 3.2.1). As mentioned, rocks' constitutive laws are among those nonlinear ones.

Another advantage is that, provided that the time step is smaller than the critical value, the material would follow a valid physical path for any type of constitutive law. Finally, since no stiffness matrixes are formed, large strain problems can be accommodated without any additional computing effort.

### 3.2.3 Limitations of the method

As mentioned in the fundamentals of the method, a small critical time step is required in order for the solution to be physically valid. This time step decreases as the element sizes decrease and also as the speed of mechanical wave propagation in the material increases. This might require numerous time step trials to get to the desired time.

Besides the time step, there is the problem of damping. Since the method solves the dynamic equation of motion, if a stable solution is desired, a damping algorithm should be introduced so that the solution stabilizes after a reasonable time. However, no significant damping algorithm which can be applied in every situation and also be realistic is introduced.

Finally, being a common issue for both implicit and explicit methods, the constitutive laws available for the rocks are very complicated and their parameters are difficult to obtain. The post-failure behavior (plasticity) is a very complicated field of study with a lot of uncertainties and questions yet to be answered [58, 59].

### 3.2.4 Conclusions

Compared to the implicit finite element methods and keeping the last two sections in mind, it is obvious that rock cutting simulations are much more suited to be performed using explicit FEM methods. They are much more efficient in the analysis of very nonlinear and large-strain problems, among which cutter-rock interaction is of specific interest here.

However, the last limitation which was pointed out regarding the complexity and non- availability of constitutive laws, significantly questions the applicability and efficiency of these methods. Not only should the rock constitutive law be the best representative of its behavior, but the contact constitutive law should also be realistic since all the interaction between the rock and the cutter is transferred through their contact. Therefore, even with the best rock constitutive law implemented, if the contact modeling is not precise, the simulation could be totally unrealistic.

With the advent of the Distinct Element Method (DEM), as explained in the following section, most of the following challenges have been overcome.

### 3.3 Distinct Element Method

#### 3.3.1 Overview

Since being first introduced by Cundall [60] in 1971, DEM has progressed and developed ever since. The major difference between DEM and FEM is the fact that DEM treats the material as a discontinuous medium, meaning the material is composed of distinct and discrete units. One can think of a material represented in a DEM model as an assemblage of discrete particles.

In a DEM, forces arise when particles overlap which are called contact forces and the magnitude of the forces is determined by the contact constitutive law. Contact forces are decomposed into two components of normal and shear forces. Usually DEM constitutive laws include normal and shear stiffness as the coefficients relating contact forces to displacements. DEM particles can also have bonds that might affect their contact stiffness and also might prevent them from separation until a determined tensile stress is developed.

Because the DEM calculation method is also explicit, it means that a critical time step according to the characteristics of the system (minimum time required for stress wave to pass from one particle to the next) is determined and dynamic equations of motion are solved for each particle and then the new contact forces are updated based on the displacements [61].

It should be mentioned that external contacts with a DEM material can also be modeled and they are sometimes called "wall" in the literature [62]. These entities could be representative of any external boundary or contact in the real world.

Friction is also specified on the contacts and controls whether the particles should undergo shear displacement or sliding.

### 3.3.2 Features of the Method

All the features mentioned in Section 3.2.2 for explicit FEM apply for DEM; however, for our purposes DEM has additional advantages.

The new approach of DEM, which considers the material as a discontinuous medium, eliminates the need for sophisticated constitutive laws developed for inherently discontinuous materials (such as rock) in FEM models. Materials represented by the basic, even linear and elastic, contact constitutive laws of DEM match the real behavior of most of the rock types far better than any FEM, even considering its highly complicated constitutive law [63].

An external contact, such as a cutter, in a DEM is dealt with the same way that the internal contacts (contacts between the particles) are being treated. No extra modeling effort and constitutive laws are required to model the contact, since the contact is an indispensable part of a DEM.

### 3.3.3 Limitations of the Method

Obviously, a material which is not inherently textured or does not have a granular structure cannot be represented by a DEM model. The major portion of the materials of engineering interest fall into this category and cannot be incorporated in a DEM model.

Being a young method, there are very limited tools available to implement a DEM algorithm in a computer, and few available codes. Because these codes are also very young and basic, limited literature is available about DEM constitutive parameters and calibrations with real materials.

### 3.3.4 Conclusions

Being compatible and coincident for rock behavior in terms of constitutive laws, great ease and flexibility in implementing external contacts (such as cutter) along with all the other advantages listed for explicit FEM methods in Section 3.2.2 and the successful works published in the literature [44, 45, 52, 54], the final conclusion was drawn that utilization of DEM would be method of choice to model cutter-rock interaction.

This chapter offered an overview that leads us to the next chapter, which is the description of the physical model and its DEM representation.

# 4 DEM Model

In this chapter the conceptual physical problem will be discussed and then the system will be implemented in the DEM model, with the details of the implementation explained in Appendix A. DEM genesis of the rock material used in the model will also be described.

## 4.1 Physical Model

The physical model is very similar to the single cutter rock interaction experimental or numerical models which were discussed before (Sections 2.2 and 2.3). However, the conditions prescribed on the cutter have a fundamental difference with the previous models. In the first subsection, the previous model will be briefly introduced, and in the second subsection, the motivations for this change will be discussed. Finally, in the last subsection, the physical model itself will be described.

### 4.1.1 Constant Depth of Cut Models

The majority of these models consist of a single PDC cutter which starts cutting the rock at a constant depth (the vertical position of the cutter is constant all over the course of simulation) while the cutter moves with a constant horizontal speed with the rock specimen held in place. Figure 4.1 illustrates a typical scenario of this model before the cutter actually starts to cut the rock. For convenience, these types of models will be termed "constant depth of cut" models.

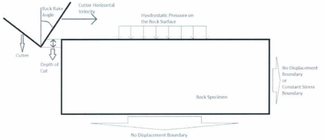


**Figure 4.1: Schematic of constant depth of cut model.**

As mentioned before, for the lateral boundaries of the model the assumption of constant stress is more realistic than the no displacement boundary (refer to Section 2.3 and also [48]). However, if the model dimensions are sufficiently large, the no displacement boundary will not affect the mechanism under investigation (rock-cutter interaction). This is why most of the models simply assume no displacement boundary conditions as the lateral boundaries.

The upper bounds of the rock (i.e., the rock surface) in most of the models are under constant hydrostatic pressure. The term "hydrostatic pressure" reflects the notion that the force vector will always be normal to the current rock surface. Therefore, if the rock surface deforms due to the action of the cutter, the force vector also changes direction so that it will still be perpendicular to the current surface geometry. This force simulates the mud hydrostatic pressure exerted on the bottom of the hole during the drilling process. The effect of mud in the rock breakage is not limited to this aspect. As mentioned in Section 2.2 and [33, 37], the filtrate of mud into the rock pore space and also pore pressure changes could also affect the failure mechanism; nevertheless, due to numerical simulation limitations, these effects have never been incorporated in the mechanical cutter-rock interaction models (to the author's knowledge).

### 4.1.2 Motivation for Changing the Boundary Conditions on the Cutter

In field drilling practices; normally, the Weight On the Bit (WOB) is controlled (or prescribed) [64] and the Rate Of Penetration (or cutter vertical displacement) is an output of the system. In the constant cutter depth simulations, in contrast, the cutter vertical displacement is fixed and the reaction forces on the cutter (an indication of WOB) are the output. The authors who made these models, back calculate the average vertical force on the cutter from the force profile resulting from the simulation output and relate that force on cutter (proportional to WOB) to the cutting depth (proportional to ROP) [44, 52, 53, 54].

This presented approach – to back calculate WOB from the output and then correlate that to ROP – works well, demonstrates good results for multiple purposes, and also matches well with experimental observations. However, for some purposes, one might be interested in evaluating and comparing the drilling response of different WOBs versus time profiles.

As an example of these situations, let us consider the case in which an oscillatory force source imposes a sinusoidal force profile in the drill string which travels down in the drill string to the bit and that sinusoidal force profile superimposes on the static WOB.

Figure 4.2 illustrates such a scenario when a hypothetical sinusoidal force source is mounted in the drill string.

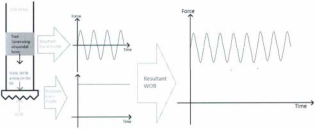


**Figure 4.2: Schematic of a hypothetic tool providing oscillatory axial force in the drill string.**

The constant cutting depth models are unable to simulate these conditions. If one aims to compare the cutting action of a conventional constant WOB drilling case to one of these scenarios, or even further, compare different frequencies and amplitudes and their relative cutting performances, the constant cut depth models fail to apply.

The Advanced Drilling Group (ADG) of Memorial University of Newfoundland has been working on design and development of such a tool (known as the "Vibration Assisted Rotary Drilling" or VARD tool) at the time of authorship. The author, as a full time graduate student working in the group, was assigned the task of developing a numerical single PDC cutter model which is capable of predicting the performance of the

VARD tool under different tool design parameters (mainly force amplitude and frequency). This was the main motivation to change the model configuration in order to investigate the desired phenomenon.

Also, the capability of such a model to predict the motion of the cutter under various loading conditions provides a valuable opportunity to investigate possible bit vibration and bit bounce.

### 4.1.3 New Model Physical Description

In the new model, the vertical force is applied on the cutter while the cutter is on top of the rock specimen. The cutter has no rotational displacement acting on it just as in the case of constant cut depth models in which the cutter has no rotational displacement. A single cutter on a PDC bit while drilling has both horizontal and vertical motions, but there is no rotation in the movement of the single cutter. After application of the vertical load on the cutter, the cutter penetrates the rock, but the real cutting process takes place when the constant horizontal velocity is prescribed on the cutter. This is when the cutter starts to slowly penetrate into the rock while a prescribed force profile is being applied on it. Figure 4.3 illustrates the described model.

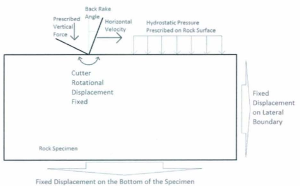


**Figure 4.3: Schematic of the cutting model.**

Other model parameters such as applied hydrostatic pressure and rock boundary conditions are essentially the same as the constant depth models which were explained in Section 4.1.1.

From here, the next section describes the DEM representation of the physical model described above.

### 4.2 DEM Model

In this section the DEM model is discussed. First the genesis of the rock specimen is explained and the rock's physical behavior will be demonstrated. Then the cutter will be added to the model and the boundary conditions will be applied.

Before proceeding, it should be pointed out that the entire modeling was based on a 2-D approach in which all the circular DEM particles have a 3-D interpretation of an extruded circle which is a cylinder. All the forces and constants are per unit thickness of these hypothetical cylinders.

### 4.2.1 Material Genesis

Generating a material specimen in a distinct element model is a process that should be done before any simulation attempt is made. Generation of specimens and all the modeling and simulations were done utilizing the commercial DEM code PFC-2D [65].

A subroutine developed in PFC-2D [66] assists in generation of a rectangular shaped rock specimen consisting of distinct particles with the DEM constitutive parameters given. The material generated and used for the purposes of this work is Carthage limestone whose DEM properties have been derived by Emam and Potyondy [73]. The results of a DEM numerical simulation of Uniaxial Compressive Stress (UCS) test on this material is calibrated with experimental test data performed on Carthage limestone [73].

The DEM material properties proposed for Carthage limestone and a brief description of their physical significance are given in the following subsection

#### 4.2.1.1 Description of Carthage Limestone DEM Properties

Density of the particles is the most important parameter as it affects the entire dynamics of the rock. The value given for the bulk density is 2620 $kg/m^3$. As mentioned, this is the density of the rock bulk and not the particle density. The material genesis subroutine is capable of generating a rock specimen of a given density.

The next two DEM parameters deal with the stiffness of the contacts between the particles. There are two parameters associated with this. Contact normal stiffness (sometimes called contact elastic constant) is given as 83 GN/m and contact shear stiffness is 21.8 GN/m. As mentioned before, normal stiffness is the normal contact force developed per unit particle overlap distance and the shear stiffness is the incremental shear force developed at the contact per unit increment of shear contact displacement.

These two parameters are tightly related to the rock elastic and shear moduli respectively.

The friction coefficient between the particles is set as 0.5. The friction coefficient determines the maximum allowable shear contact force that can be developed based on the normal contact force.

$$F_{s,max} = \mu F_n \tag{4.1}$$

Where $F_{s,max}$ is the maximum allowable contact shear force and $\mu$ is the friction coefficient and $F_n$ is the normal contact force. The friction coefficient is tightly related to the friction angle, for example in Mohr-Coulomb failure criteria (see Section 2.1)

To simulate the effect of cement bonding material grains together, additional normal and shear stiffness values are defined in the model and they act in parallel to the contact stiffness values. (Therefore, they simply add to the stiffness values of contacts). In the DEM, these are called parallel bonds and the values given for them are the same as the values of contact stiffness (i.e., 83 GN/m for normal and 21.8 GN/m for shear stiffness).

The parallel bonds, simulating the effect of cement between the material grains, break if one of the following two criteria is met: i) Shear contact force exceeds the parallel bond shear strength, or, ii) normal contact force exceeds the parallel bond tensile strength. Once a parallel bond is broken, their stiffness is no longer effective in the contact behavior. Parallel bonds allow tensile forces to develop between particles as long as they exist, exactly like the real cement holding the material grains.

The values of contact bond shear and tensile strengths are not constant for all the particles in the proposed material model. They follow a normal distribution over all particles. The mean values for both parallel bond shear and tensile strength are given as 91.0 MN and the standard deviation is given as 20.0 MN for both. The material tensile strength is a strong function of its parallel bond tensile strength.

The particle sizes follow a normal distribution with the ratio of 1.66 of maximum particle size to the minimum particle size. In order to have a fully defined particle size distribution DEM model of the rock, in addition to the maximum to minimum particle size ratio, the minimum (or maximum) particle size should also be determined; however, this parameter is not strictly determined. Different types of Carthage limestone might be comprised different grain sizes; although, demonstrating the same behavior in terms of the rest of their DEM parameters.

Figure 4.4 shows that for a specimen generated with minimum particle size of 1 mm, the specimen size is 100 x 50 mm.

**Figure 4.4: Generated specimen, normally distributed particles from the minimum size of 1mm to maximum of 1.66 mm. Specimen dimensions are 50 mm wide and 100 mm tall (generated using material genesis module).**

#### 4.2.1.2 Carthage Limestone DEM Model Testing and Verification

PFC/2-D provides a tool to simulate a UCS test on a generated specimen and monitor stresses and strains on the specimen. This makes calibration and verification of the generated material with experimental data for the UCS test possible.

As mentioned in the last section, there is one DEM parameter in the Carthage limestone model which is not determined strictly and is optional. In fact, in the sedimentation and lithification process of limestone, depending on the type of the sedimentary basin in which the limestone is formed, the average grain size and their distribution might vary.

A series of simulated UCS tests were performed to obtain values of Young's modulus and Poisson's ratio and UCS values for a material represented by the DEM properties described in Section 4.2.1.1 and various particle sizes.

Samples with 50x100 mm dimensions with minimum particle sizes ranging from 0.2 mm to 1.4 mm were subjected to simulated UCS tests. Figures 4.5 and 4.6 show the obtained Young's modulus and Poisson's ratio values versus minimum particle size respectively.

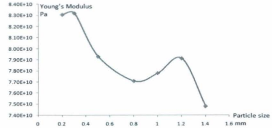


**Figure 4.5: Obtained Young`s modulus versus minimum particle size (data point are generated using the material genesis module).**

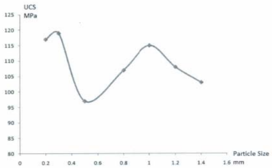


**Figure 4.6: Obtained UCS value versus minimum particle size (data points are generated using material genesis module).**

Table 4.1 shows the values obtained for Young's modulus and Poisson's ratio and UCS and compares them to experimental tests values given for Carthage limestone [67].

**Table 4.1: Physical properties obtained from different minimum particle sizes and also experimental test values (data points are generated using material genesis module).**

| Min Part. Rad. | Young's Modulus, Gpa | Poisson's Ratio | UCS, Mpa |
|---|---|---|---|
| 0.2 | 83.1 | 0.29 | 117.00 |
| 0.3 | 83.2 | 0.29 | 119.00 |
| 0.5 | 79.3 | 0.27 | 97.00 |

| | | | |
|---|---|---|---|
| 0.8 | 77.1 | 0.32 | 107.00 |
| 1 | 77.8 | 0.30 | 115.00 |
| 1.2 | 79.1 | 0.28 | 108.00 |
| 1.4 | 74.8 | 0.29 | 103.00 |
| Experimental | 76 | 0.29 | 100 |

No monotonic trend is found in the answers, which demonstrates that rock macro-properties are complicated functions of rock micro-properties (DEM parameters). Nevertheless, as a rule of thumb, it can be stated that the finer the rock particles are, the higher their compliance and their strength most likely to be, all the other micro-properties kept the same.

The closest match between the experimental data given for Carthage limestone [67] and DEM models is the rock with minimum particle size of 1.4 mm. This does not mean that the others do not describe a Carthage limestone, but for that specific rock sample a minimum particle radius size of 1.4 mm is considered to be the most appropriate one (this is a relatively high particle size for sedimentary rocks).

Figure 4.7 shows the state of the specimen with minimum particle radius of 0.3 mm at the end of the simulated UCS test. Both red and blue lines indicate broken parallel bonds between the particles, red lines mean that parallel bond is broken due to tensile failure and blue lines means that the parallel bond is broken due to shear failure (see section 4.2.1.1).

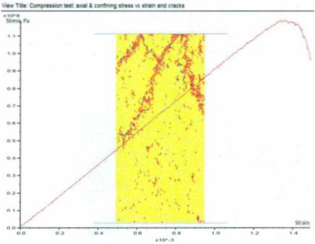


**Figure 4.7: State of the specimen under simulated UCS test after failure and associated stress-strain curve (generated using the material genesis module).**

Usually, in experimental UCS test, one or two major cracks develop which propagate from one end of the specimen to the other. Here, in this simulated test, it can also be observed that a major crack (accumulation of broken parallel bonds) is formed from one end and propagates up towards the specimen top where the second major crack is initiated and propagated down to the other side of the specimen. Therefore, the two cracks could be thought of as one single crack propagating from one side to the other. As if the specimen was long enough, it would probably propagate in the same path to the other side without reflecting back from the boundary. This cracking pattern which produces conically shaped samples after failure has been observed in experimental UCS tests numerously.

As a conclusion, the material defined by the DEM parameters described in section 4.2.1.1, represents a material whose behavior matches the experimental observations with very good accuracy.

#### 4.2.2 Cutter in DEM model

The cutter is a rigid body that consists of extremely small DEM particles. In PFC/2-D these sets of particles which do not move relative to each other are called "clumps" [68]. The purpose of clumps is mainly to create DEM particles of arbitrary shapes and to simulate materials whose particles are shaped far from even an approximation of a circle.

As mentioned, the clump particles do not move relative to each other and therefore no contact forces develop between them. This clump logic was utilized to construct a rigid cutter in these simulations.

The main physical properties of the cutter in terms of its DEM parameters are described in this section.

As illustrated in Figure 4.3, the cutter initially sits on top of the rock specimen. One of the main properties of the cutter is its rake angle. The face of the cutter is not necessarily perpendicular to the rock specimen surface. Sometimes called "cutter back rake angle", this property is proved to be very influential in drilling performance (see Sections 2.2 and 2.3 and [16, 21, 27]). Refer to Section 2.2 for the definition and more detailed terminology related to rake angle from a bit point of view. From a cutter point of view, rake angle is simply the angle of deviation of the cutter front face from the vertical line.

The cutter angle is also another parameter to be set. Most of the PDC cutters have an angle very close to 90 degrees. In Figure 4.3, the cutter angle is also 90 degrees.

In these types of models, the cutter friction coefficient is the most influential physical parameter of the cutter. In a DEM model, as explained in Section 4.2.1.1, the friction coefficient is the factor that controls maximum allowable shear contact force developed between two DEM elements. In the same loading on the cutter regime, a cutter with a higher friction coefficient is more likely to experience higher horizontal force values.

Values for friction coefficient for the bit are reported by Kuru [69], and range from 0.07 to 0.15 depending on the rock type. The DEM value of cutter friction could be higher than these values since all these experiments were based on the assumption that the cutter has already met the maximum shear criteria (see Section 4.2.1.1).

The cutter is a rigid body in this model, therefore there is no compliance or elastic modulus is required for it. The assumption of rigid body is completely reasonable since the elastic modulus and also UCS values of PDC are several orders of magnitude higher than those of rock.

The model is described and all the main parameters are explained in this chapter. The mutual dependence of DEM model parameters and their physical meanings are explained.

This introduces us to the next chapter which is a detailed discussion of input model parameters and their physical significance in terms of real drilling operations.

## 5 Model Input Parameters

This chapter deals with those input parameters of the model, in which the sensitivity of the drilling operations to them are of primary interest. Interpretation of the meaning of those parameters in terms of real drilling operations is included.

### 5.1 Prescribed Vertical Force on Cutter

As described in the physical model in Section 4.1.3, a vertical force is applied (prescribed) on the cutter and this is the major difference of this model compared to others in which displacement on the cutter is prescribed. In Section 4.1.2, it was clearly explained why this scenario of loading is more realistic and also how it can simulate certain loading conditions that the previous models are not capable of.

The question arises that the force on the cutter corresponds to what parameter in real field drilling? The answer is Weight on Bit (WOB), the famous drilling parameter which is always given to the driller by the drilling designer or engineer to maintain a certain WOB.

Weight on the bit is provided by the drilling hoisting system [64], which consists of the drilling strings (including drill collar and drill pipe) in the upper end of the rig that are connected to a hook. The hook applies an adjustable amount of upward force to the drill string, which counteracts the downward force resulting from the weight of drill strings, and the resultant force (after accounting for buoyancy effect due to drilling fluid density) is applied on the bit and is called WOB.

Changing the hook load causes equivalent changes in WOB, and the driller at any time is able to change the hook load to supply the desired WOB.

Calculation of forces applied on each individual cutter for typical PDC cutters is possible, but is complicated and needs solid design software coupled with finite element methods. Typical PDC cutters have complicated 3-D spatially distributed cutters. Despite these complications, for the goals and motivations of our research (see Section 4.1.2), which is mainly a comparative study of the performance of a tool which is a dynamic force source, it is quite reasonable to assume that a force profile of the same nature that is applied to the bit will also be transmitted to the cutter. For example, consider a situation in which a 10 kN force is applied on the bit and 1 kN of this force is on a certain cutter.

Then a hypothetical oscillating force on the bit is added, with an amplitude of 2 kN and a frequency of 100 Hz. In the exact same way that 10% of 10 kN force on the cutter was applied to the cutter, 10% of this force will be applied on the cutter as well, which is force oscillation with 0.2 kN amplitude and 100 Hz frequency. Therefore, the superimposed force oscillation on the whole bit with an amplitude of 20% of the constant force is transmitted to an oscillatory force profile on the cutter with the same ratio of amplitude to constant force on the cutter.

A simple instance of the forces on a single cutter for a very simple and small designed PDC bit shown in Figure 5.1 is discussed below. The bit is the property of Advanced Drilling Group of Memorial University of Newfoundland.

**Figure 5.1: 2 PDC cutter bit view from different angles (figure in the left is top view). Bit dimensions : Bit diameter 36 mm, Total Length 60 mm.**

The PDC cutters are clearly visible from the figures. This simply designed PDC bit with two cutters, which despite its simplicity is very efficient, has a diameter of 50 mm. The picture in the middle shows the rake angle of one of the PDC cutters. Since the cutters are symmetric and their tips are on the same horizontal plane, under ideal conditions the vertical force on each cutter is half of the full WOB exerted on the bit.

However, this is not always the case for typical PDC bits in which cutters are positioned non-symmetrically either from a side view or top view. Complicated force and moment balance equations might be needed to solve geometries with even a small number of PDC cutters. Figure 5.2 shows another simple PDC bit with 5 cutters. Even if all the cutters had a tip lying on the same horizontal plane, the arrangement of the cutters from the top view is not symmetric and the moment balance equation (even for static case of loading, without bit rotation) will result different forces on individual cutters.

**Figure 5.2: A more complicated PDC bit configuration (also a property of the Advanced Drilling Group). Bit dimensions: bit diameter 55 mm, bit length 125 mm.**

An applied weight on the cutter of 10 kN in reality will translate to almost 1000 kN/m (= 10 kN/cm) of force for a 2-D DEM model, since the model assumes a unit thickness of the cutter (1 m) for the forces to be applied, while the PDC cutter as viewed in the 2-D model is extruded from the 2-D plane with almost 1 cm. (The typical thickness of the PDC cutters are in this order of magnitude.)

### 5.2 Prescribed horizontal velocity on Cutter

The horizontal velocity applied to the cutter simulates the rotary action of the bit. As the bit rotates around its axis, the cutters travel a circular path as viewed from the top. The reason why horizontal velocity is being applied and not the horizontal force is because the rotational speed, rather than torque, is prescribed on the drill string (and consequently the bit). In 2-D, the circular path being traveled by the cutter is simplified into a straight path and therefore the circular motion of the cutter will translate into a linear velocity.

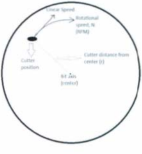


**Figure 5.3: Interpretation of horizontal cutter speed for individual cutters of a full PDC bit.**

For a PDC cutter with a distance of r from the bit center and a rotary speed of N RPM, the linear velocity to be used in the 2-D single cutter model is determined using Equation 5.1.

$$V_H = {}^{\pi}/_{30}\ N.r \tag{5.1}$$

Where $V_H$ is in meters per second and r is in meters.

Depending on the position of the cutter on the bit, the horizontal velocity will be different for different cutters on the same bit. The bigger the radial distance of the cutter, the more accurate the approximation of a circular travel path with a linear path (because the curvature of a circle is the inverse of its radius).

A question that might arise is, how does this model simulate the performance of a cutter which is positioned exactly on the bit center? Secondly, will the horizontal speed be zero? The answer is that, to the author's knowledge, no PDC bit has a cutter placed exactly on the center and all of the cutters on a PDC bit have an offset distance from center (however small). For example, consider the two simple PDC bits shown in section 5.1. Nevertheless, let us consider a hypothetical PDC bit which has a cutter exactly on the center, with the thickness of the cutter represented by t and the vertical force on the cutter identified by F. The author's proposed approach to model this cutter is to approximate its action by two separate cutters as shown in Figure 5.4.

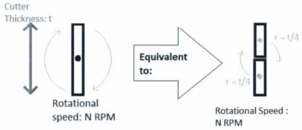


**Figure 5.4: Approximating behavior of a hypothetical cutter located in the bit center with two separate cutters.**

The cutter behavior is approximated by two cutters traveling with a horizontal speed of $^{\pi}/_{120}\ N.t$ and with an applied vertical force of F/2 on each cutter. However, in a 2-D model since the vertical force is expressed per unit thickness, the magnitude of the force will still remain the same (assuming the vertical force is distributed symmetrically on the cutter).

### 5.3 Hydrostatic Pressure on the Rock Surface

As mentioned for the physical model (Section 4.7), a force with hydrostatic nature is applied on the rock specimen's upper surface. The hydrostatic force means that the force is always perpendicular to the current surface of the rock; therefore, if the rock deforms, the direction of the force will change accordingly to account for the modified geometry.

A detailed description of the algorithm used in identification of the rock surface and application of the pressure on it is described in the manual of PFC/2-D [66]. Note, however, that the use of the clump logic in these simulations slightly changes the algorithm of finding the rock surface. A brief description of this change can be found in Appendix A.

There is mud column hydrostatic pressure, which is exerted on the rock surface in the bottom of the hole, where cutters are in contact with the rock. The amount of this pressure depends on the True Vertical Depth (TVD) [64] of the well being drilled and also the density of the drilling mud being used. TVD refers to the vertical component of the well depth, which is essentially the same as well depth for the case of vertical wells. Equation 5.2 shows the relationship between mud hydrostatic pressure and these drilling parameters.

$$Hydrostatic\ Pressure = (Mud\ Density) * (Gravitation\ Acceleration) * (TVD) \tag{5.2}$$

Therefore, this DEM model parameter corresponds to the drilling depth and also the drilling mud density.

### 5.4 Lateral Specimen Boundaries

The boundaries of the model, as explained in the physical model description (section 4.1.3), are no displacement boundaries, which could be considered a misleading term in a DEM model. To be more precise, the lateral and bottom boundary of the specimen are made by mounting stationary "walls," which are another DEM entity besides particles and clumps. Particles in contact with the wall are able to move towards the wall and a contact force between the particles and the wall forms due to this motion. Walls have a specified stiffness, which is usually defined as several orders of magnitude higher than those of particles, and therefore, very small motions of the particles take place at the proximity of the walls. Resultantly, the term "no displacement boundary" is a good description of such boundaries.

As mentioned in the physical model description, a more realistic assumption for the lateral boundary conditions of the rock specimen is to apply constant lateral stresses on the boundary. This will be more representative of the real stress state of the geological formations encountered at depth [48]. At the time of writing of this thesis, this boundary condition was not implemented in the model; however, the implementation is easy and is planned to be done in future model modification plans. This represents the far-field formation stresses that develop in the geological time scale and are functions of depth and rock density and tectonic history[48].

# 6 Model Output Parameters and their Physical Interpretation

In this chapter, the outputs of the model are discussed, the method of their calculation is explained, and their significance in terms of drilling operational parameters is presented.

## 6.1 Cutter Tip Penetration

In this section, the single cutter interpretations extracted from cutter tip penetration profiles are provided, and then a simple full PDC bit model developed on the basis of the parameters introduced for a single cutter scenario.

### 6.1.1 Single Cutter Interpretations

As mentioned before, the main difference between this model and the previous cutter rock interaction models is that it takes the force on the cutter as its input and outputs the resultant cutter penetration into the formation.

The interpretation of the penetration profile from the simulation is a big topic of discussion itself. It is not, as it was believed initially, just the measurement of the rate of cutter tip penetration inside the rock.

To have a sense of what a typical penetration profile looks like, Figure 6.1 shows the state of rock cutting 0.125 seconds after the cutting simulation started.

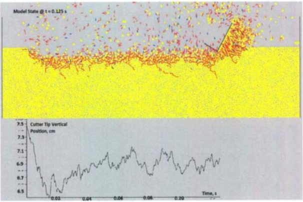


**Figure 6.1: State of the model at t = 0.125s, and cutter tip vertical position versus time. The cutter tip vertical position is measured from the middle of the specimen.**

In this specific simulation, the minimum particle size is 1 mm, and the cutter is moving with a horizontal speed of 2 m/s. The vertical force on the cutter is set at 1 MN, which means that 1 MN of force is applied per 1 meter thickness of the cutter. (For a cutter thickness of 1 cm, this translates into 10 kN vertical force on the cutter.) No pressure is applied on the rock surface.

Taking a look at the graph of penetration of the tip into the rock (Figure 6.1), a rapid high speed penetration of the cutter tip inside the rock is noticeable. This rapid high speed penetration takes 15 milliseconds, and after that the cutter continues advancing without any more penetration, and it starts to oscillate around a mean depth. The initial penetration rate (rapid penetration zone) is 0.7 m/s; such a penetration speed is several orders of magnitude higher than typical penetration speeds measured in field (<0.001 m/s). This parameter obviously does not represent the ROP achieved by the cutter.

Looking at the illustration of the system and the graph, it can be seen that the cutter starts to maintain a certain mean cut depth after its initial rapid penetration. Therefore, such a loading regime, despite the initial hypothesis of the author, does not cause a uniform penetration of the cutter tip inside the rock. It makes the cutter maintain a certain (average) depth of cut after an initial rapid penetration. A slightly upward trend of the cutter tip penetration might be noticed, but the author speculates that this slight decrease in the overall cutter tip depth is due to the effect of failed particles piled up in front of the cutter. In reality a constant depth of cut is maintained.

Several types of treatments can be made on the outcome of the cutter penetration profile. One is to simply average the penetration values over time. This function, as given in Equation 6.1, is the integration of the penetration values over time per unit of time.

$$\overline{Ct}(t) = \frac{\int_0^t Ct(t)\,dt}{t} \tag{6.1}$$

In this equation, $Ct(t)$ is the instantaneous penetration at time t, i.e. cutter vertical tip position from the specimen upper boundary at time t. $\overline{Ct}(t)$ is the function describing the average cut depth at time t.

Figure 6.2 shows the graph of average cut depth with time for the same system illustrated in the beginning of this section.

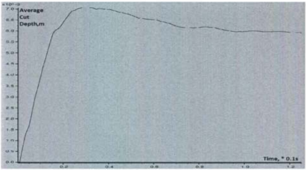


**Figure 6.2: Average cut depth versus time.**

As it can be seen from the figure, the average cut depth increases to a maximum (at approximately 7 mm) and then starts decreasing smoothly before appearing to become asymptotic to a certain final average cut depth (approximately 5.7 mm). This final value is the most important kinematic representation of the cutter behavior and it will be called "final cut depth" throughout the remainder of this thesis. It is represented by $\overline{Ct_f}$ .

Changing the rock cutting environment operational parameters definitely changes the value of final cut depth; however, the general trend and behavior of the cutter penetration remains the same, which is a rapid penetration of the cutter inside the rock and then a consistent average cut depth through the rest of the process.

For the same cutter and rock properties, the final cut depth is a function of vertical force, horizontal velocity, and bottomhole pressure as shown in Equation 6.2.

$$\overline{Ct}_f = \overline{Ct}_f(F, V_H, BHP) \tag{6.2}$$

Where F is the force on the cutter (expressed per unit thickness of the model), $V_H$ is the horizontal velocity and BHP is the pressure on the rock specimen surface.

Another parameter which might be interesting and physically meaningful is called the "material removal rate" or MRR. Equation 6.3 shows MRR as a function of time in terms of average cut depth:

$$MRR(t) = \overline{Ct}(t).V_H\,.Thickness \tag{6.3}$$

Having the units of volume per time, this quantity shows the average rate of rock volume cut at any time during the cutting process. By defining the average material removal rate on the basis of final cut depth, Equation 6.4 is proposed:

$$MRR_f = \overline{Ct}_f\,.V_H\,.Thickness \tag{6.4}$$

Where $MRR_f$ is the average material removal rate. The exact same functionality of Equation 6.2 is valid for MRR as well.

The author proposes that measurement and comparison of relative performance of different loading scenarios should be done by comparing either the final cut depth or the average MRR together.

In the next subsection, the parameters defined here will be used in conjunction with a simple full PDC bit model to demonstrate one proposed method of predicting field ROP values using single PDC cutter tests.

### 6.1.2 PDC Bit Design and Single Cutter Test Results

As was previously mentioned, the typical PDC bits being used in the industry are very complicated in the design, as well as the geometric and spatial distribution of the cutters.

However, based on some simplified bit design parameters, this section is an attempt to relate the results of single cutter tests to the PDC bit performance, and particularly ROP.

The material discussed in this subsection, to author's knowledge, has not been referenced before and is based on a completely theoretical PDC bit model in an attempt to relate results of single cutter test to actual field drilling ROP based on the bit design. The defined parameters might not be defined anywhere else and might not even be a real PDC bit design parameter that is used by bit manufacturer companies since they do not reveal their design criteria and parameters. The whole intention of this discussion is to be a starting point for such studies (if any).

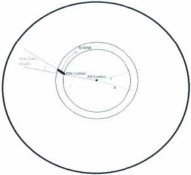


**Figure 6.3: A single PDC cutter as viewed from top on a PDC bit.**

Certainly, there is not just one PDC cutter on the bit face. Let us assume that each PDC cutter on the face of the bit has a unique identification number starting from 1 to M where M represents the total number of cutters on the bit. The numbering does not necessarily have to be done in any order as long as all the cutters are numbered.

Figure 6.3 shows the top view of a PDC bit with one single cutter shown for illustration purposes. Let us assume that the ID number for this cutter is i. According to definition in some literature [e.g. 27], side rake angle is defined as the angle between PDC cutter and the line perpendicular to the PDC cutter motion direction (i.e., radius). In one rotation of the bit, the cutter removes a ring shaped portion of the rock (as viewed from top) with small radius of $r_i$ and big radius of $R_i$. The relationship between $r_i$ and $R_i$ is given in Equation 6.5:

$$R_i = r_i + T_i \cos(\lambda_i) \tag{6.5}$$

Where $T_i$ is the diameter of the PDC disc and $\lambda_i$ is the side rake angle.

For the purpose of bit design assessment, assume a hypothetical thin ring-shaped area with small diameter of $\hat{r}$ and a thickness of $d\hat{r}$. The parameter $O_i$ is defined as the amount of overlap that the hypothetical ring makes with the ring made by the circular motion of cutter. If no portion of these two rings overlaps, then $O_i$ is simply zero.

The horizontal linear speed (in order to be input into the single cutter model) for the cutters lying in the ring can be calculated as $N.\ \pi.(\hat{r} + \frac{d\hat{r}}{2})\ /30$.

If the forces on the individual cutters, based on the total force on the bit (WOB), are given so that $F_i$ relates to the force on PDC cutter i, considering the functionality described in the single PDC analysis for MRR, we can derive an expression relating total material removal rate for the cutters present in the hypothetic ring-shaped area.

$$MRR = \sum_{i=1}^{M} \left[ \overline{Ct}_f \left( \frac{F_i}{T_i}, N\pi\left(\hat{r} + \frac{d\hat{r}}{2}\right)/30, BHP \right) * O_i * N\pi\left(\hat{r} + \frac{d\hat{r}}{2}\right)/30 \right] \tag{6.6}$$

The function $\overline{Ct}_f$ is the output of single cutter simulations as explained in the last section and Equation 6.2. The subscript 'i' for each variable refers to that parameters associated with the ring with ID number 'i'.

An expression for ROP can be derived at this point since the rate of penetration is the rate of material removal divided by the area under which the material is removed. In this case (assuming a relatively thin ring) this area is $\hat{r}d\hat{r}$. Therefore, Equation 6.7 is derived for ROP:

$$ROP = \sum_{i=1}^{M}\left[\overline{Ct}_f\left(\frac{F_i}{T_i}, N\pi\left(\hat{r}+\frac{d\hat{r}}{2}\right)/30, BHP\right) * O_i * N\pi\left(\hat{r}+\frac{d\hat{r}}{2}\right)/(30\hat{r}d\hat{r})\right] \qquad (6.7)$$

This equation relates the depths of cuts which are outputs of a single cutter simulation to the ROP. Note that this ROP value is derived on the basis of the performance of the cutters laying on the hypothetical ring area described before. However, a properly designed bit should have a cutter arrangement designed in such a way that the ROP values derived for each ring are equal. Otherwise, the bit will bounce and become unstable until a new stable force distribution is reached by the cutter. For clarity, a stable force distribution means equal resultant ROP values were calculated for different rings.

Figure 6.4 shows the hypothetical ring superimposed on an image of a typical PDC bit. The PDC cutters that lie on the ring either full or partially are indicated by a crossmark.

**Figure 6.4: An illustration of the hypothetical ring used in derivation of ROP for full bit.**

It should be noted that, for simplicity's sake, the PDC cutter faces are assumed to be rectangular in these calculations; however, in reality they are circular. Also, if the intention is just to calculate the ROP, there is no need to necessarily consider a ring for the calculations. It would probably be easier to take the whole cutters and calculate the total cutters' MRR and then divide it by the total bit area to get the ROP. But if the objective is to investigate bit stability and validate the appropriateness of the bit design, the ring approach should be considered.

### 6.2 Energy Related Variables

#### 6.2.1 Single Cutter Energy Variables

As pointed out in the literature review in Sections 2.2 and 2.3, the parameter called drilling Mechanical Specific Energy is an even more important criterion than ROP to predict the drilling performance. Drilling Mechanical Specific Energy is defined as the energy consumed by the drilling system to remove a unit volume of rock. This parameter can be defined in several ways for the case of single cutter testing and each definition has its own interpretation.

The total energy transmitted by the cutter to the rock at any time t, referring to elapsed time since the start of a cutting process, is given by Equation 6.8:

$$ME(t) = \int_0^t (F_x V_x + F_y V_y)\, dt \tag{6.8}$$

Where F is the force applied on the bit and V is bit velocity in the x and y directions, which are horizontal and vertical directions respectively. ME(t) is the mechanical energy or the total energy transmitted by the drilling system. The calculation of this factor is a simple numerical integration done by a function that inputs the forces and velocities of the cutter every few cycles of simulation and adds the new summation over this time step to the previous value of ME.

The typical behavior of this quantity is an approximately linear increase with respect to drilling time. The reason for the linear increase is probably due to the constant horizontal speed of the cutter, while the horizontal force oscillates around a nearly constant mean.

Considering the two terms in Equation 6.8, it is obvious that the total energy could be decomposed to its two components: the energy delivered by the horizontal movement of the cutter, and the energy delivered by the vertical force applied to the cutter. The relationship between these terms is not immediately obvious; however, the author assumes that the ratio of these two terms should be equal for both single cutter testing and field drilling.

Another parameter defined is the specific energy per current penetration, which is simply the ratio of ME(t) to the current cutter penetration (time t). Rather than being a reliable parameter of drilling efficiency, this is more of a measure of rock strength and compliance. It shows how much energy is consumed to attain the current amount of penetration, and does not take the removal of material into account. The author does not recommend utilization of this parameter in any interpretation.

A more reliable specific energy parameter is defined as ratio of ME(t) to average material removal rate at time t multiplied by t.

$$MSE(t) = \frac{ME(t)}{MRR_f.t} \tag{6.9}$$

This parameter will give the amount of energy consumed to remove a unit volume of material by the cutter, also known as Mechanical Specific Energy (MSE). Figure 6.5 shows mechanical specific energy per unit penetration and total mechanical specific energy versus time.

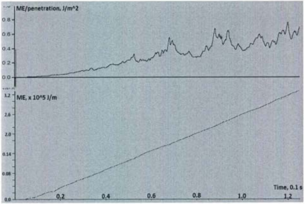


**Figure 6.5: Mechanical energy per unit penetration and total mechanical specific energy.**

The Mechanical Specific Energy increases and then stabilizes around a certain value after the cut depth is stabilized. The initial low values of MSE are due to easy initial penetration of the cutter and low horizontal force exerted on the cutter during the period of rapid penetration. (Note that the graph in the figure is not the MSE, although its graph looks similar). The horizontal force profile with respect to time for the same system is shown in Figure 6.6.

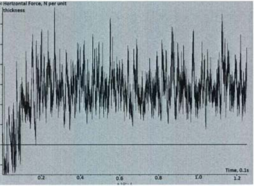


**Figure 6.6: Horizontal force on cutter versus time.**

A net negative horizontal force is acting on the cutter for the first 10 milliseconds. The reason is that the cutter is being pushed forward by the mostly intact rock surface, which is in contact with the back of the cutter, since the cutter has not advanced significantly forward and no part of rock is in direct contact ahead of the cutter. The cutter during this small period of time (as explained in the interpretation of single cutter tip penetration in Section 6.1.1) is mostly trying to attain the stabilized depth of cut. After reaching to the approximately constant depth cut region, as demonstrated in the graph, the horizontal force oscillates around a constant value. The reason for the high amplitude fluctuations in the profile, as believed by the author, is due to relatively large grain size which causes sudden application or release of horizontal load on the cutter front face upon the bond failure.

### 6.2.2 Full Bit Energy Variables

The model developed for the full PDC bit in Section 6.1.2 can be used for energy considerations as well. In order to apply the same type of model for the whole specific energy response of the bit, we need to define another parameter. As shown in Figure 6.6, the horizontal force on the cutter stabilizes around a specified mean value for each rock cutting scenario. The same functionality of depth of cut, as suggested in Equation 6.2, is valid for this parameter as well. Therefore, the following statement can be written:

$$\overline{F_H} = \overline{F_H}\,(F, V_H, BHP) \tag{6.10}$$

Where $\overline{F_H}$ is the average horizontal force value attained after cutter depth stabilization. The functionality parameters were previously defined in Equation 6.2.

To write the expression for energy consumed by each individual cutter in terms of the newly introduced term, average horizontal force, we can safely neglect the vertical force component of the energy term. The reason is that there is just a small portion of time in which the cutter is actually having a considerable vertical velocity (the rapid penetration zone) but towards the rest of the simulation, the cutters maintain an approximately constant depth, which means that the vertical component of the force accounts for a very small and almost negligible portion of the total energy. Therefore the following equation can be written for the energy of an individual cutter i:

$$ME_i(t) = \overline{F_{Hi}}\left(\frac{F_i}{T_i}, N\pi\left(r_i + \frac{T_i\cos(\lambda_i)}{2}\right)/30, BHP\right) * V_H * \mathrm{t} / \mathrm{T_i} \tag{6.11}$$

The division by $T_i$ is made to convert the force given by the model (per unit thickness) to the real horizontal force acting on the cutter since its thickness is known.

Summation of all these energy values for all the PDC cutters on the bit will give us the total energy consumed.

$$ME_{full\ bit}(t) = \sum_{i=1}^{M} \overline{F_{Hi}}\left(\frac{F_i}{T_i}, N\pi\left(r_i + \frac{T_i \cos(\lambda_i)}{2}\right)/30, BHP\right) * V_H * t/T_i \quad (6.12)$$

Using the expression derived for ROP in section 6.2.2 and also taking the bit radius to be $R_{bit}$ the following equation will give us the mechanical specific energy.

$$MSE_{full\ bit}(t) = \frac{ME_{full\ bit}(t)}{\pi . R_{bit}^2 . ROP.t} \quad (6.13)$$

It is appropriate to conclude this section by noting that this full bit model development is in an early stage, and contains many simplifying assumptions. Realistically, the MSE represented by Equation 6.13 is the maximum MSE since each single cutter is assumed to be cutting a completely fresh rock and does not account for the damage caused by adjacent cutters. Therefore, any utilization of this method should be done with caution.

### 6.3 Crack History

As discussed in Section 4.2.1.1 for the DEM material properties of Carthage limestone, parallel bonds exist between the particles in the material. These bonds add to the contact stiffness and also allow tensile stresses to develop between grains. This simulates the behavior of cement in real granular materials.

Failure or breakage of a parallel bond between the grains creates a crack or a broken bond. Once the bonds between two particles are broken, the additional contact stiffness on the rock is no longer effective. This additional contact stiffness works in parallel with the contact stiffness and sometimes is called parallel bond stiffness. Although, it is noteworthy that the particles can still develop normal and shear stresses between themselves.

The number of broken parallel bonds and their mode of failure (shear or tensile) over the course of the simulation is another output parameter of interest. Although it is not as directly evident and measurable as other parameters, such as depth of cut and mechanical energy, it does provide potentially useful output from this simulation regarding the mode of failure and location of macroscopic cracks and morphology of the cuttings generated by the drilling process. An instance of their usefulness is demonstrated below.

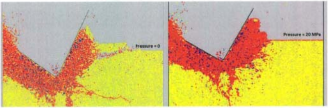


**Figure 6.7: Two different crack patterns for low and high pressure environments.**

Figure 6.7 shows the states of two simulations: one without the presence of bottomhole pressure and the other with 20 MPa pressure on the rock surface. Red marks denote locations of parallel bond failed in tension and blue marks are those of shear bond failure. An analysis of these two figures reveals the mode and nature of rock breakage in high and low bottomhole pressures. For example, a very clear continuation of parallel bond failure up to the surface of the rock specimen in the figure on the left (no pressure) shows that a macroscopically visible crack forms at that region which separates a chip of the rock from the main body of the rock. The parallel bonds inside the chip are not broken; therefore, the failure takes place by chipping and is also called a brittle failure. This failure type is considered to be the most effective and efficient type of failure. Note that even though the cracks forming the chip are tensile in a microscopic and granular point of view, the macro crack is considered to be a shear crack in a full scale study which agrees with the relative motion of the fracture sides once displacement occurs. The mode of inter-granular bond failure and the developed macroscopic crack do not necessarily have to be the same.

On the other side of the figure, the high pressure environment, a pile up of particles whose contacts have been broken is formed which is pushed towards the cutter by the high hydrostatic pressure applied on its surface. Because there is no apparent crack and no chip formed, it seems that the cutter has to overcome and break every single parallel bond between the particles in order to move forward. This contrasts the low pressure case, where the cutter easily advances without the need to break all the parallel bonds. This the high pressure failure mode is similar to what is sometimes called ductile failure.

A zone of crushed rock (groups of rocks with broken contact bonds) is formed underneath the cutter for both cases. If this zone of rock forms in reality, it is definitely easier for the next cutter to drill than a fresh virgin rock surface and even this zone is a little bigger in the case of low pressure than the other (the figures have the same scale). Aside from the geometric pattern of the developed cracks, the history of the number of cracks formed versus the time of simulation could also be another output of interest.

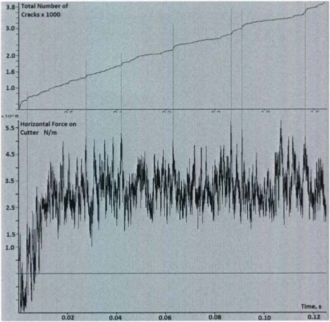


**Figure 6.8: Graphs of horizontal force on cutter and total cracks formed versus time.**

As an example, graphs of horizontal force on the cutter and total cracks formed are shown in Figure 6.8. Orange lines connect the times when the horizontal stress reaches its local peak, and at the same time it can be seen that the total number of cracks starts to increase suddenly. Those are the times that the horizontal movement of the cutter requires a cluster of parallel bonds to break altogether. The author believes that (as explained in Section 6.2.1) the high amplitude fluctuations in horizontal force and also sudden jumps in crack formation is due to size of the rock particles; and the finer the particles, the smoother the process.

This subsection introduced the main outputs of the model and their physical and practical significance. In the next chapter, some simulation results are presented. At the time of preparation of this thesis, simulation results were limited. However, a few simulations were done previously and the results were published by the author of this thesis elsewhere [70]. These are presented in the next chapter.

# 7 Some Preliminary Simulation Results

The following two subsections are taken directly from the paper authored by the author of this thesis and his thesis supervisors [70]. Please note that the output parameters introduced and proposed in Sections 6.1 and 6.2 were not investigated at the time of authorship of this paper (which also coincides the time of preparation of this thesis). The cutter dynamics and ROP are not introduced by the parameters proposed in Section 6.1.

The initial speed of penetration (denoted as the "rapid penetration period" in Section 6.1) was the topic of analysis, and the term ROP in this section refers to this factor and not the one defined in Section 6.1. The focus of the simulations is to assess the performance of VARD style drilling as described in Section 4.1.2 as the main motivation of this new cutter-rock interaction model.

## 7.1 Results for VARD drilling with no Bottomhole Pressure

A set of four simulations on a rock sample with dimensions of 100 cm by 100 cm were conducted. No hydrostatic pressure was applied to the rock surface. One simulation was performed with constant weight on cutter $WOB_{static}$ and the other three were with variable weight on cutter around a mean value equal to WOB but with superimposed variable forces of an amplitude of $0.2*WOB_{static}$ and frequencies of 300, 600, and 1000 Hz respectively. All the other cutting parameters were kept constant. Therefore the general force profile is as follows:

$$WOB(t) = WOB_{Static}(1 + Psin(2\pi ft)) \tag{7.1}$$

Where P is the amplitude of oscillation divided by $WOB_{static}$ and f is oscillation frequency.

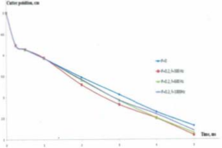

**Figure 7.1: Cutter tip penetration.**

Figure 7.1 shows the cutter tip position for four different drilling scenarios, in which the highest amount of penetration has taken place in the case of 300 Hz oscillation and the lowest is for the case of conventional drilling simulation. There is about an 8% increase in rate of penetration by adding force oscillations with a frequency of 300 Hz.

Increasing the frequency to 600 and 1000 Hz causes a decrease in penetration rate; therefore, there will be an optimum frequency (lower than 300 Hz) which would result in the maximum penetration rate for this particular oscillation amplitude. A comprehensive study to clarify ROP behavior with oscillation frequency and inclusion of rock visco-elastic parameters and resonating behavior is underway.

Another monitored factor is the number of tensile and shear cracks for each case. The number of shear and tensile cracks formed at the end of 5 ms of simulation is shown in Table 7.1.

**Table 7.1: number of cracks for each case at the end of 5 ms.**

| | Shear Cracks | Tensile Cracks | Total Cracks |
|---|---|---|---|
| P=0 | 2200 | 15900 | 18100 |
| p=0.2, f=300Hz | 2300 | 19000 | 21300 |
| p=0.2, f=600Hz | 2000 | 16300 | 18300 |
| p=0.2, f=1000Hz | 2250 | 18600 | 20850 |

Again, for the 4 cases tested, the number of cracks formed are maximum for the case of 300 Hz oscillation and minimum for the case of conventional rock cutting. They can be correlated to the number of particles which are free to be removed since the contact bond is removed. It might not immediately affect the rate of cutter tip penetration inside the rock but the authors believe that it will affect the drilling efficiency and penetration rate in the long run.

Another important factor reflects the instabilities and vibrations induced by the cutting process. Vibrations imposed on a drill string as a result of rock-bit interaction has been identified as one of major areas of concern in drilling safety. Interaction with certain rocks might cause huge bit bounces and drill string vibrations. Force oscillation superposition on the cutter does not necessarily mean an increase in the amount of vibrations in drill string.

A thorough investigation of these vibrations is being carried out. A Fourier analysis will be made on instantaneous ROP vs. time data to extract vibration characteristic of different cutting scenarios, and identify and delineate hazardous drilling conditions for different rock types.

One preliminary result is that the larger the rock average grain size, the larger the amplitude of vibrations regardless of loading condition. Also, there is a certain optimum frequency in which the vibrations minimize (and in fact, diminish) even compared to conventional drilling for each rock type.

For the case of the described four scenarios, without performing a Fourier analysis it can be stated that all the cases have a smooth penetration without any significant vibration observed. However, in the case of 1000 Hz force oscillations small vibrations with a frequency of about 1000 Hz but an amplitude of less that 0.01mm can be observed by studying the plot of Figure 7.2. This does not suggest any specific trend in the induced vibrations with WOB and is just an example of how different a rock response could be depending on loading condition (Figure 7.4).

Figure 7.2 shows the state of cutting at t=1.1 ms. In the case of 300 Hz oscillations we can see that two major and relatively large sized cuttings are about to form. The crushed zone is being referred to the zone close to cutter which has a red color. Rock grains in these zones are crushed and detached from each other. The smallest cutting belongs to the case of no force oscillation as it can be clearly seen from the picture.

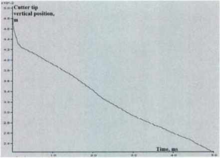


**Figure 7.2: Cutter penetration history for p=0.2, f=1000 Hz.**

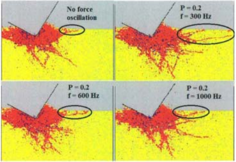


**Figure 7.3: State of four simulations at t = 1.1 ms, potential cuttings are being circled.**

In addition to the cutting size, the damage propagation is much deeper and larger for the case of 300 Hz oscillation (the zone of crushed rock). The volume of rock removed under no borehole pressure conditions and perfect cleaning efficiency is the total volume of cuttings and rocks in crushed zone.

### 7.2 Results for VARD drilling in Presence of Bottomhole Pressure

In order to make a preliminary investigation on the influence of bottomhole pressure in rock cutting process, another factor was added to the model. This factor is a hydrostatic pressure applied to the rock upper surface to simulate the effect of mud hydrostatic pressure in deep drilling environments. However, in real drilling conditions the mud exerts a drag force on the bottomhole as it exits nozzle jets which is not accounted for in the applied hydrostatic force.

Two sets of simulations run for the case of no force oscillation and 300 Hz oscillation, each with four different bottomhole pressures. Two important results were produced.

The first result is that the rate of penetration decreases linearly as the logarithm of bottomhole pressure increases. The best fitting equation to the data obtained from the no force oscillation simulation is shown below.

$$ROP = -0.11\ \log(BHP) + 7.12 \tag{7.2}$$

All the units are SI and BHP is the acronym for bottomhole pressure. Please refer to the notes of the start of this section for some clarification regarding the term ROP in this context, since it is completely different with the ROP defined previously defined. It should be taken into consideration that the weight on cutter does not change as the bottomhole pressure changes, while in reality as the well becomes deeper usually weight on the bit increases. A similar equation is extracted for the case of 300Hz oscillations.

$$ROP = -0.11\ \log(BHP) + \frac{0.51}{\log(BHP)} + 7.12 \tag{7.3}$$

The new term introduced into Equation 7.3 shows that the effect of force oscillation diminishes as the bottomhole pressure increases. As in this case, an 8% increase for the case of no bottomhole pressure decreases to almost 2% increase with a bottomhole pressure of 2 MPa. Figure 7.4 shows these results with 10 data points at 5 different pressures.

The results of these simulations were also observed experimentally by DRI [71].

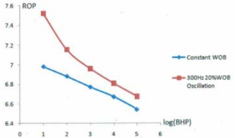


**Figure 7.4: Effect of bottomhole pressure on rate of penetration.**

The exact reason of this phenomenon is not yet completely understood; however, the authors believe that the oscillating force produces extra bond breakage energy into the system which is the same for both the cases of with and without pressure. Therefore, that same amount of energy will produce much less damage to the rock as the bottomhole pressure increases.

# 8 Future Work

The work described in this thesis is a continuation of a series of interconnected previous works and builds upon the framework of that literature. Expansion and further verification of this ongoing investigation is necessary and this chapter briefly proposes the modifications and additions that can be done for this work.

## 8.1 Adding Cleaning Efficiency Factor

One limitation is that the model does not account for the cleaning efficiency of the cutting action whatsoever. All the simulations are done with no bottomhole cleaning efficiency.

In a comparative study in which the bottomhole cleaning efficiency of the hydraulic system is not the factor under study, these simulations give the desired results since the cleaning efficiency is the same for all the cutting states. However, if the interest is specifically on the effect of bottomhole cleaning or its impact and interaction with other drilling parameters, this should be added to the model.

One possible scenario is to simply delete a certain percentage of the particles which all their parallel are failed and calling this percentage the cleaning efficiency percentage. This is the simplest way to implement a cleaning efficiency logic to this simulation.

Other options are also envisioned; for example computational fluid dynamics considerations coupling the mechanical system with the mechanics of the fluid exiting the nozzles of the PDC bit will give some indications of the efficiency of the hydraulic system in cutting removal.

### 8.2 Pore Pressure Considerations

As mentioned in section 2.2 and [33, 36] the formation virgin pore pressure could sometimes be as important as the bottomhole pressure itself especially in low RPM drilling and high permeability rocks. This effect is not included in the model and the code that is utilized does not have the ability to simulate this effect.

Modification of the DEM code written in order to accommodate this pore pressure effect, however basic in its calculations, in simulation cycles could resolve many ambiguities.

### 8.3 Wear Measurement Using Coupled Thermal Analysis

Cutter wear rate is a key factor in the evaluation of drilling performance and determines the drilling overall cost when considered in parallel with rate of penetration [64].

It has been hypothesized that the PDC cutter wears out in accordance with either a mechanical or thermal failure criterion. Coupled thermal analysis in a DEM model is possible using basic heat transfer laws and friction loss-thermal coupled analysis. The results of the analysis in series with the mechanical and thermal failure criteria will give measures of the cutter wear rate.

## 8.4 More Advanced Scenarios

Full bit rock interaction analysis using the results of the single cutter, and eventually making a 3-D DEM model and making a direct full bit simulation, could be a realistic plan in the near future plan to add sophistication to these studies.

Coupled analysis of the response of the rock on the bit and the interaction of drill bit-drill string using FEM analysis methods will give insight into the performance of the drilling system on a much larger scale, and may reveal the possible interactions between the rock characteristics and drill string dynamics.

# 9 Concluding Remarks

Single PDC cutter rock interaction models demonstrate their significant potential in solving the full bit rock interaction problems and to provide insight into the nature of rock failure caused by PDC bit action. Experimental and numerical simulations of this process have given fairly similar results further confirming the validity of both approaches.

Evaluation of cutting performance of different bits and also different drilling systems (from a loading viewpoint) is much easier numerically and could save a lot of resources before utilization of those systems.

As a small, but important and complex unit of the whole drilling system, the cutter rock interaction models can be coupled with other models of the drilling system such as the drillstring model and fluid circulation system model to result in a unified simulation of the drilling system as a whole.

It is confirmed that the single cutter models relying on constant depth of cut are not capable of reproducing the effect of down-the-hole tools generating oscillatory force profiles and therefore, they are not useful for evaluation of the VARD tool performance.

On the other hand the model relying on penetration of the cutter inside the rock is sensitive to different force on the cutter profiles and can give a good insight of the performance of VARD (and similar) tools.

The simulations show that each cutting simulation gives a mean value of the depth of cut which is a function of the main input parameters. In the same way, they show that each cutting simulation gives a mean value for horizontal force on the cutter around which the instantaneous value of the horizontal force on the cutter oscillates.

The first parameter explained above (mean cut depth) is the main variable of all the functions which tend to relate the output to ROP and the second parameter (mean horizontal force) is the main variable of all the functions which tend to relate the output to MSE.

Another unique feature of the present model compared to the previous constant depth of cut models is the fact that (as explained above) the two output parameters ROP and MSE are determined independently and they are associated with two independent outputs. In the constant depth of cut models, the MSE is being determined by the output (mean horizontal force) but the ROP is being determined by an input of the system (depth of cut).

To be more rigorous, there is another feature for the present model which the previous models are not capable to produce. The MSE is composed of the energies consumed by the horizontal and vertical components of the force on the cutter. The constant depth of cut models do not have the vertical component of cutter movement in their energy terms since the cutter does not have a velocity in the vertical direction. In the present model, both terms are included and the MSE is calculated as the addition of both components. It has been shown that the energy consumed by the vertical component of the force is much less than the other component either in reality or in the simulation that were conducted with the new model.

In terms of VARD style drilling in low pressures, author speculates from the simulations that were done, the drilling performance generally increases by the introduction of a VARD tool in the drill string. There is a certain frequency of force oscillations for each set of drilling input parameters in which the maximum efficiency of cutting (in terms of cutting size and ROP) is achieved which might be a function of the natural frequency of the rock.

In terms of VARD style drilling in high pressures, the same observations are valid; however, the intensity of the efficiency of the VARD tool diminishes by increase in pressure. The main reason for this is a fundamental change in the failure mode (brittle to ductile) of rock while going from low pressure to high pressure zones.

## References


[1] N. Saabyeottosen and M. Ristinmaa. *The Mechanics of Constitutive Modeling*. Elsevier Science, The Netherlands, 2005.

[2] G.T. Houlsby. "A General Failure Criterion for Frictional and Cohesive Material." *Soils and Foundations*, vol. 26, no. 2, pp. 97-101, 1986.

[3] R.T. Fenner. *Mechanics of Solids*. Blackwell Scientific Publications, Oxford University Press, 1989.

[4] C.G. Li, X.R.Ge, H. Zheng and S.L. Wang. "Two-Parameter Parabolic Mohr Strength Criterion and Its Damage Regularity." *Key Engineering Materials,* vol. 306 - 308, Fracture and Strength of Solids VI, pp. 327-332, 2006.

[5] J.B. Cheatham.. "Indentation analysis for rock having a parabolic yield envelope." *International Journal of Rock Mechanics and Mining Sciences & Geomechanics Abstracts*, vol.1, Issue 3, pp. 431-436, 1964.

[6] R. Hill. *The Mathematical Theory of Plasticity*. Oxford University Press, USA, 1998

[7] D. C. Drucker and W. Prager. "Soil mechanics and plastic analysis for limit design." *Quarterly of Applied Mathematics*, vol. 10, no. 2, pp. 157–165, 1952.

[8] Unlisted. "Standard Test Method for Unconsolidated-Undrained Triaxial Compression Test on Cohesive Soils" USA. ASTM D2850 - 03a, 2007.

[9] E. Fjaer, R.M. Holt, P. Horsrud, A.M. Raeen and R. Risne. *Petroleum Related Rock Mechanics*. Elsevier Science, The Netherlands, First Edition, 1992

[10] K. Hashiguchi. "Generalized plastic flow rule." *International Journal of Plasticity*, vol. 21, Issue 2, pp. 321-351, 2005.

[11] D.C. Drucker. "Some implications of work hardening and ideal plasticity." *Quarterly of Applied Mathematics*, vol. 7, pp.144-418, 1950.

[12] V. Racherla."Non-associated plastic flow and effects on macroscopic failure mechanisms" Ph.D Dissertation, University of Pennsylvania, USA, 2007.

[13] D.H. Zeuch and J.T. Finger."Rock Breakage Mechanisms With a PDC Cutter," presented at the 60th Annual Technical Conference and Exhibition of the Society of Petroleum Engineers, Las Vegas, NV, USA,1985.

[14] G. Hareland and P. R. Rampersad."Darg - Bit modeling including wear," presented at the Latin American/Caribbean Petroleum Engineering Conference, Buenos Aires, Argentina, 1997.

[15] P.N. Jogi, W.A. Zoeller and E. Teleco. "The Application of a New Drilling Model for Evaluating Formation and Downhole Drilling Conditions," presented at the Seventh SPE Petroleum Computer Conference, Houston, TX, USA,1992.

[16] R.H. Knowlton." PDC Bits Using Positive Rake Cutters," presented at the SPE/IADC Drillling Conference, Houston, TX, USA, 1990.

[17] S.M. Behr, T.M. Warren, L.A. Sinor and J.F. Bret. "3-D PDC bit model predicts higher cutter loads."*SPE Drilling and Completion*,vol. 8, no. 4, 1993, pp. 253-258.

[18] D.H. Zijsling. "Single Cutter Testing - A Key for PDC Bit Development," presented at the Offshore Europe, Aberdeen, UK, 1987.

[19] D.A. Glowka."Use of single cutter data in the analysis of PDC bit designs: Part 1__Developement of a PDC cutting force model." *Journal of Petroleum Technology*, vol. 41,no. 8, pp. 797-849, 1989.

[20] T.M. Warrena and A. Sinor. "Drag bit performance modeling," presented at the SPE Annual Technical Conference and Exhibition, New Orleans, LA, USA,1986.

[21] M. Ghoshouni and T. Richard,."Effect of back rake angle and groove geometry in rock cutting," presented at the ISRM International Symposium - 5th Asian Rock Mechanics Symposium, Tehran, Iran, 2008.

[22] G. Hareland, W. Yan, R. Nygaard and J. L. Wise."Cutting Efficiency of a SinglePDC Cutter on Hard Rock. " *Journal of Canadian Petroleum Technology*, vol 48, no. 6, pp. 60-65, 2009.

[23] R. Nygaard and G. Hareland."Calculating Unconfined Rock Strength from Drilling Data," presented at the 1*st* Canada-U.S. Rock Mechanics Symposium, Vancouver, BC, 2007.

[24] W. Yan. "Single PDC Cutter Force Modeling for Hard Rock Cutting." Ph.D. dissertation, New Mexico Institute of Mining & Technology, Socorro, NM, 1997.

[25] L. Gerbaud, S. Menand and H. Selami."PDC Bits: All comes from the cutter/rock interaction," presented at the IADC/SPE Drilling conference, Miami, FL, USA, 2006.

[26] H. Sellami. "Simulation du travial d'un pic : modelisation de la phase de penetration," DEA Ecole des Mines de Paris, 1984.

[27] C. Coudyzer and T. Richard."Influence of the back and side rake angles in rock cutting,"presented at the AADE 2005 National Technical Conference and Exhibition, Wyndam, Houston, TX, 2005.

[28] E. Detournay and P. Defourny."A phenomenological model for the drilling action of drag bits." *International Journal of Rock Mechanic and Mining Science & Geomechanic Abstracts,* vol. 29, no. 1, pp. 13-23, 1992.

[29] C. Fairhurst and W.D. Lacabanne. "Hard Rock Drilling Techniques." *Mine and Quarry Engineering* ,vol. 23, pp.157-161, 194-197, 1957.

[30] N. Rafatian, S. Miska, L.W. Ledgerwood, R. Ahmed, M. Yu, and N. Takach. "Experimental study of MSE of a single PDC cutter interacting with rock under simulated pressurized conditions,"SPE/IADC Drilling Conference and Exhibition, Amsterdam, 2009.

[31] R. Simon."Energy balance in rock drilling." *SPE Journal*, vol. 3. no. 4, pp. 298-306, 1963.

[32] R. Teale."The concept of specific energy in rock drilling." *International Journal of Rock Mechanics and Mining Science*, vol. 2, no. 5, pp. 57-73, 1967.

[33] E. Detournay and C. Atkinson. "Influence of pore pressure on drilling response of PDC bits" presented at the 32nd U.S. Symposium on Rock Mechanics (USRMS), Norman, OK, USA,1991.

[34] M.E. Merchant. "Basic mechanics of the metal cutting process." *Journal of applied mechanics,*vol. 11,pp. 168-175, 1944.

[35] M.E. Merchant. "Mechanics of metal cutting process I. Orthogonal cutting and a type 2 chip." *Journal of Applied Physics* ,vol. 16, no. 5, pp.267-275, 1945.

[36] S. Saeb and B. Amadei. "A mathematical model for the shear behavior of a dilatant rock joint", presented at the 31th U.S. Symposium on Rock Mechanics (USRMS), Golden, CO, USA, 1990.

[37] B. Peltier, C. Atkinson. "Dynamic Pore Pressure Ahead of Bit." *SPE Drilling Engineering*, vol. 2,no. 4, pp. 351-358, 1987.

[38] K. Terzaghi. *Theoritical soil mechanics*. Wiley, New York, 1943.

[39] E. Fjaer, R.M. Holt, P. Horsrud, A.M. Raeen and R. Risnes."Failure Mechanics" in *Petroleum Related Rock Mechanics*, Elsevier Science, The Netherlands, First Edition, 1992.

[40] E. Victor, M.J. Kleinosky. "Finite element simulation of rock cutting : a fracture mechanics approach," presented at theThe 25th U.S. Symposium on Rock Mechanics (USRMS), Evanston, IL,USA,1984.

[41] J. Pierry, R. Charlier. "Finite element modeling of shear band localisation and application to rock cutting by a PDC tool," presented at the Petroleum Engineering Conference, Delft, The Netherlands, 1994.

[42] J.R. Rice."The localization of plastic deformation." *Proceedings of the14th International Congress on Theoretical and Applied Mechanics*, Delft, 1976, pp. 207-222.

[43] X.C. Wang, R. Charlier and J. Pierry. "Numerical modeling of a rock cutting process," presented at the ISRM 8 Congress, Tokyo, Japan, 1995.

[44] H. Huang, E. Detournay and B. Bellier. "Discrete element modeling of rock cutting." *Informatyka w Technologii Materiałów*, vol. 7, no. 2, pp. 224-230, 2007.

[45] Q.M. Gong, J. Zhao and H.Y. Sian."Numerical simulation of influence of joint orientation on rock fragmentation process induced by a TBM cutter." *Tunneling and Underground Space Technology,* vol. 20, Issue 2, pp. 183-191, 2005.

[46] G. Han and M.S. Bruno. "3-D simulation of rock breakage with air hammers in gas well drilling," presented at the 2006 SPE Gas technology symposium, Calgary, AB, Canada, 2006.

[47] P.L. Guarin, H.E. Arnold, W.E. Harpst and E.E. Davis. "Rotary percussion drilling." *Drilling and Production Practice,* pp. 112-122, 1949.

[48] I.M. Breckles and V. Eekelen."Relationship between horizontal stress and depth in sedimentary basins." *Journal of Petroleum Technology*, vol. 34, no. 9, pp. 2191-2199, 1982.

[49] G. Han and M. Bruno."Percussion drilling, from laboratory tests to dynamic modeling", presented at the 2006 SPE International Oil and Gas Conference and Exhibition, Beijing, China, 2006.

[50] I.B. Tulu , K.A. Heasly, I. Bilgesu and O. Sunal."Modeling rock and drill cutter behavior", presented at the 42th U.S. rock mechanics symposium and 2nd U.S.-Canada rock mechanics symposium, San Francisco, CA, USA, 2008.

[51] I.B. Tulu , K.A. Heasly ."Calibration of 3-D cutter-rock model with single cutter tests", presented at the 43th U.S. Rock mechanics symposium and 4th U.S./Canada rock mechanics symposium, Ashville, NC, USA, 2009.

[52] G. Block and H. Jin. "Role of failure mode on rock cutting dynamics", presented at the 2009 SPE annual technical conference and exhibition, New Orleans, LA, USA, 2009.

[53] M.C. Jaime, I.K. Gamwo, D.K. Lyons and J.S. Lin. "Finite element modeling of rock cutting", presented at the 44th U.S. Rock mechanics symposium and 5th U.S./Canada Rock mechanics symposium, Salt Lake City, UT, USA, 2010.

[54] J.A. Mendoza, I.K. Gamwo, W. Zhang and Lin J.S. "Discrete element modeling of rock cutting using crushable particles", presented at the 44th U.S. Rock mechanics symposium and 5th U.S./Canada Rock mechanics symposium, Salt Lake City, UT, USA, 2010.

[55] A.F. Bower. "Theory and Implementation of the Finite Element Method" in *Applied Mechanics of Solids*, 1st edition, USA: CRC, 2009.

[56] R. Hill. "Path sensitivity of material response at intrinsic eigenstates in classical plasticity." *Mathematical Proceedings of the Cambridge Philosophical Society*, vol. 103, Issue 2, pp. 317-381, 1988.

[57] P.A. Cundall. "Explicit Finite Difference Methods in Geomechanics." *Proceedings of the EF Conference on Numerical Methods in Geomechanics*, Blacksburg, VA, 1976, pp. 132-150.

[58] R.O. Davis and A.P.Selvadurai. *Plasticity and Geomechanics*. Cambridge, 2002.

[59] P.A. Vermeer and R. de Borst. "Non-Associated Plasticity for Soils, Concrete and Rock." *Heron*, vol. 29, no. 3, pp. 3-64, 1984.

[60] P.A. Cundall. "A Computer Model for Simulating Progressive Large Scale Movements in Blocky Rock Systems." *in Proceedings of the Symposium of the International Society of Rock Mechanics,*Nancy, France, 1971, pp. 213-216.

[61] P.A. Cundall. "Distinct Element Models of Rock and Soil Structure" in *Analytical and Computational Methods in Engineering Rock Mechanics*. E.T. Brown, Ed. London: Allen & Unwin, 1987, pp. 129-163.

[62] Unlisted. *PFC2-D Theory and Background*. Minneapolis, MN: Itasca Consulting Group Inc., 2008.

[63] S. Hentz , F.V. Donze´ and L. Daudeville. "Discrete element modelling of concrete submitted to dynamic loading at high strain rates." *Computers and Structures,*vol. 82, pp. 2509–2524, 2004.

[64] A.T. Bourgoyne, K.K. Millheim, M.E. Chenevert and F.S. Young."Drilling Hydraulics" *in Applied Drilling Engineering,* First Printing. Richardson, TX, USA: SPE 1986.

[65] PFC-2D Version 4.0, Minneapolis, MN, USA : Itasca Consulting Group Inc., 2008.

[66] Unlisted,"PFC Fishtank" in *PFC-2-D", FISH in PFC*, Forth Edition. Minneapolis, MN, USA: Itasca Consulting Group Inc.,2008, pp. 33-58.

[67] D.O. Potyondy and P.A. Cundall. "A Bonded-Particle Model for Rock." *International Journal of Rock Mechanics and Mining Science*, vol. 41,no. 8, pp. 1329–1364, 2004.

[68] Unlisted, *PFC-2-D Theory and Background*. Minneapolis, MN, USA: Itasca Consulting Group Inc., 2008.

[69] E. Kuru and A.K. Wojtanowicz."An experimental study of friction induced by PDC cutters during rock cutting," presented at the CIM 1992 Annual technical conference, Calgary, AB, Canada, 1997.

[70] B. Akbari, S.D. Butt, K. Munaswamy and F. Arvani. "Dynamic Single PDC Cutter Rock Drilling Modeling and Simulations Focusing on Rate of Penetration Using Distinct Element Method," presented at the 45th US Rock Mechanics / Geomechanics Symposium, San Francisco, CA, 2011.

[71] J.V. Pennington. "Some results of DRI Investigations- Rock Failure in Percussion." *Drilling and Production Practice,* pp. 329-336, 1953.

[72] W.C. Maurer. "The perfect-cleaning theory of rotary drilling." *Journal of Petroleum technology*, vol. 14, no.11, pp. 1270-1274, 1962.

[73] S. Emam, D. Potyondy. "Internal Technical Memorandum — PFC2D Rock-Cutting Procedures" Internet: http://www.itascacg.com/pdf/pfc/ex_rockcut2d.pdf, August 11, 2011.

# Appendix A: An Overview of Implementing the Model in PFC-2-D

The model development in PFC-2-D is described in this appendix.

The very first step to start the modeling this process is to generate the rock specimen. Below, the input code from which the rock specimen is generated is presented. The codes shown here are PFC input files. The description flows in the order in which the code is written in the actual model input file.

```
set logfile D-spc.log
set log on
; ------------------------------------------
 new
 set safe_conversion on
 SET disk on  ; model unit-thickness cylinders
 SET echo off  ; load support functions, Loading the functions for
material genesis
   call %fist%\fist_new.dvr
   call %fist%\2-D_3-D\md_setup.fis
   call D-param.dat
   call %fist%\2-D_3-D\md.fis
   call %fist%\2-D\et2.fis
   call %fist%\2-D_3-D\flt.fis
   call %fist%\2-D_3-D\crk.fis
   call %fist%\2-D\chl.fis

 SET echo on
```

```
SET md_run_name='D'
title 'D-spc'  ; Setting up the parameters required for material
genesis
  SET random 10001
  SET mg_Rmin=1e-3  ; Nb=800 (20 x 2 x 20)
  SET mv_H=50e-3  mv_W=300e-3
  SET mg_quiet=0
mg_matgen
```

The first few lines call the necessary functions from the standard PFC function library (Fishtank), and in the last lines the specimen dimensions and material minimum particle radius are specified. The very last line calls the material genesis function from Fishtank and the material is generated.

A simple function which returns the maximum ball (=particle) ID in the system is next. This is done in order to know what ball ID should be the starting ball ID of the clump which is going to represent the cutter.

```
def FindMAxBallID
bp = ball_head
FindMaxBallID = 0
loop while bp # null
if b_id(bp)>FindMAxBallID then
FindMaxBallID = b_id(bp)
end_if
bp = b_next (bp)
```

```
end_loop
end
```

Finding the maximum ID of the balls in the current system, the cutter which is made of a clump will be made.

```
def MakeACutterClump
; Inputs: RakeAngle, BallRadSize, CutterLength, StartPoint,
CutterFrictionCoefficient
TipID = FindMaxBallID + 1000
CutterFrictionCoefficient = CutterFrictionCoefficient
counter = 0
loop while counter<CutterLength/(BallRadSize*2)   ; Making the right
side of the cutter, Starting ID is 1000 higher than the maximum ball id
in the current system
XLoc = (-StartPoint * mv_W * 0.5 + sin(RakeAngle*3.14/180) * 2 *
BallRadSize * counter)
YLoc =  (0.5*mv_H + BallRadSize*4 + cos(RakeAngle*3.14/180) * 2 *
BallRadSize * counter )
BallID = TipID + counter
command
ball density 2620 rad=@BallRadSize x @XLoc  y @YLoc  id @BallID
property kn 1e22 ks 1e22 fric @CutterFrictionCoefficient range id
@BallID
end_command
counter = counter + 1
end_loop
RightCutterTopBallID = BallID
StartID = TipID + counter -1
```

```
counter = 1
FirstCutterLeftBallID = StartID + counter
loop while counter<CutterLength*0.5/(BallRadSize*2)   ; Making the left
side of the cutter
BallID = StartID+counter
XLoc = (-StartPoint * mv_W * 0.5 - cos(RakeAngle*3.14/180)* 2 *
BallRadSize * counter)
YLoc = (0.5*mv_H + BallRadSize*4 + sin(RakeAngle*3.14/180) * 2 *
BallRadSize * counter )
command
ball density 2620 rad @BallRadSize id @BallID x @XLoc  y @YLoc
property kn 1e22 ks 1e22 fric @CutterFrictionCoefficient range id
@BallID
end_command
counter = counter + 1
end_loop
FinalCutterBallID = BallID
ClumpStartY = mv_H / 2
ClumpEndY = ClumpStartY + mv_H
command
clump add id 1 range y @ClumpStartY @ClumpEndY
end_command
TotalNumOfBallsInCutter = RightCutterTopBallID - TipID +
FinalCutterBallID - FirstCutterLeftBallID + 2
TotalMassOfCutter = TotalNumOfBallsInCutter * 3.14 * BallRadSize *
BallRadSize * 2620
end
```

The function 'MakeTheChains' whose code is presented below, attempts to form a chain by calling the 'chain' function from Fishtank library in a loop of attempts starting from the highest ball in the cutter face (the clump is made of balls), and if the algorithm fails, the ball next to the previous ball is tried. The algorithm is shown to be robust and is able to make the chain to apply the pressure on it. The difference between this code and the one available for rock cutting in the Fishtank library is that in that code there is no need to try different balls in a loop, the cutter is made of a single entity called wall and one attempt is enough. The main difference is that forces cannot be specified on the walls in PFC. The same procedure is followed for the back of the cutter, and a second chain is made there.

```
def MakeTheChain
cs_clearmarks
BallID = RightCutterTopBallID
ch_num = 1
ch_cw = 1
ch_sort = 0
section
  loop while BallID > (TipID - 1)
    ch_s0 = find_ball(BallID)
    ch_s1 = find_wall(4)
    if cs_spanchain = 0 then
       ch_s1 = find_wall(1)
    end_if
    if cs_spanchain = 1 then
```

```
      exit section
    end_if
    BallID = BallID - 1
  end_loop
endsection
if BallID = (TipID - 1) then
  error = 'Could not form spanning chain in front of the cutter'
end_if

BallID = FinalCutterBallID
ch_num = 2
ch_sort = 0
ch_cw = 1

section
  loop while BallID > (FirstCutterLeftBallID-1)
    ch_s0 = find_wall(3)
    ch_s1 = find_ball(BallID)
    if cs_spanchain = 1 then
      exit section
    end_if
    BallID = BallID - 1
  end_loop
  BallID = TipID
  loop while BallID < (RightCutterTopBallID + 1)
    ch_s0 = find_wall(3)
    ch_s1 = find_ball(BallID)
```

```
    if cs_spanchain = 1 then
      exit section
    end_if
    BallID = BallID + 1
  end_loop
endsection
if BallID = (RightCutterTopBallID + 1)
  error = 'Could not form spanning chain in back of the cutter'
end_if
end
```

This Function is called every determined number of model cycles which is given by the user defined variable 'pressrate'

```
def chain
; INPUT: pressrate
  chain_cnt = chain_cnt + 1
  if chain_cnt = pressrate then
    command
      SET update_contacts on  ; ensure contact geom will be okay next
cycle
    end_command
  else
    if chain_cnt > pressrate then
      MakeTheChain
      command
        SET update_contacts off
```

```
      end_command
      chain_cnt = 0
    end_if
  end_if
end
```

This function itself is defined as a 'fishcall' which is called every cycle after calculation of motion of particles with the dynamic equation of motion.

Total horizontal force on the cutter is calculated by summation of horizontal components of the force on the individual cutter balls. The function written for it is shown below.

```
def TotalTorqueOnCutter
  NormalForceSum = 0
  ShearForceSum = 0
  NormalForceSumV = 0
  ShearForceSumV = 0

  loop bid (TipID,RightCutterTopBallID)
    bp = find_ball (bid)
    cp = b_clist ( bp )
    loop while cp # null
      fac = 1.0
      if c_ball1(cp) = bp then
        bp_other = c_ball2(cp)
        cpnext = c_b1clist(cp)
```

```
      fac = -1.0
    else
      bp_other = c_ball1(cp)
      cpnext = c_b2clist(cp)
    end_if
    if b_id(bp_other)<TipID then
      NormalForceSum = NormalForceSum + fac * c_nforce(cp)*c_xun(cp)
      NormalForceSumV = NormalForceSumV + fac * c_nforce(cp)*c_yun(cp)
      ShearForceSum = ShearForceSum + fac * c_sforce(cp)*c_xun(cp)
      ShearForceSumV = ShearForceSumV + fac * c_sforce(cp)*c_yun(cp)
    end_if
    cp = cpnext
  end_loop
end_loop

loop bid (FirstCutterLeftBallID,FinalCutterBallID)
  bp = find_ball (bid)
  cp = b_clist ( bp )
  loop while cp # null
    fac = 1.0
    if c_ball1(cp) = bp then
      bp_other = c_ball2(cp)
      cpnext = c_b1clist(cp)
      fac = -1.0
    else
      bp_other = c_ball1(cp)
      cpnext = c_b2clist(cp)
```

```
      end_if
      if b_id(bp_other)<TipID then
        NormalForceSum = NormalForceSum + fac * c_nforce(cp)*c_xun(cp)
        NormalForceSumV = NormalForceSumV + fac * c_nforce(cp)*c_yun(cp)
        ShearForceSum = ShearForceSum + fac * c_sforce(cp)*c_xun(cp)
        ShearForceSumV = ShearForceSumV + fac * c_sforce(cp)*c_yun(cp)
      end_if
      cp = cpnext
    end_loop
  end_loop

  TotalTorqueOnCutter = -(NormalForceSum + ShearForceSum)
  TotalVerticalForceOnCutter = NormalForceSumV + ShearForceSumV

  VerticalUnbalanced = TotalVerticalForceOnCutter + ForceToApply

end
```

Finally, the function called 'cut' is defined which does the actual cutting. It sets the required Fishcalls and sets the movie and saves it, and also saves the state of the simulation in predefined intervals. It also integrates MSE and ME during cycling and makes the necessary changes in the force applied on the cutter or bottomhole pressure or horizontal velocity defined for the cutter if they are defined as an oscillatory function.

```
def cut ; inputs: MeanVerticalForce, TotalDisp, Percent, frequency,
TotalSaves
```

```
command
  clump property yforce @MeanVerticalForce  range id 1
  set fishcall #FC_CYC_MOT MakeVacuum
end_command
crk_init
FixClumpAngular
command
  SET PLOT AVI size 1024 768
  MOVIE AVI_OPEN   file D_ct.avi
  MOVIE STEP 1000 4 file D_ct.avi
  cycle 1000
end_command
FixCutterVelocity
initialLoc = cl_x (clp)
ch_init
command
  set fishcall #FC_CYC_MOT chain
end_command
SaveNo = 1
InitialYLoc = b_y(find_ball(TipID))
loop while SaveNo < (TotalSaves + 1)
  loop while (cl_x(clp)-initialLoc) < SaveNo*(TotalDisp/TotalSaves)
    ForceToApply = Percent * MeanVerticalForce * 0.01 * sin ( 2 * 3.14 *
frequency * time ) + MeanVerticalForce
    PressureToApply = MeanPressure + PPercent * MeanPressure * 0.01 *
sin ( 2 * 3.14 * Pfrequency * time )
    StartTime = time
```

```
    cl_xvel(clp) = HorizontalVelocity + LPercent * HorizontalVelocity *
0.01 * sin ( 2 * 3.14 * Lfrequency * time )
    command
      set ch_press = PressureToApply
      clump property yforce @ForceToApply range id 1
      cycle 20
    end_command
    StopTime = time
    TorqueEnergy = TorqueEnergy + (TotalTorqueOnCutter * cl_xvel(clp)) *
(StopTime - StartTime)
    WOBEnergy = WOBEnergy + (ForceToApply * cl_yvel(clp)) * (StopTime -
StartTime)
    CutterEnergy = TorqueEnergy + WOBEnergy
    Penetration = InitialYloc - b_y(find_ball(TipID))
    MSE = CutterEnergy / Penetration
;    CalcDisp   ;==> HERE the integration is performed while cycling
  end_loop
  md_run_name = 'ModelState '
  md_tag_name =  string(SaveNo) + 'from' + string(TotalSaves)
  md_save_state
  SaveNo = SaveNo + 1
end_loop



command
  MOVIE AVI_CLOSE file D_ct.avi
```

```
end_command
end
```

For more information regarding the coding concepts of PFC please refer to the software manuals